

An Evaluation of Surface Wind and Gust Forecasts from the High-Resolution Rapid Refresh Model

Robert G. Fovell and Alex Gallagher

Department of Atmospheric and Environmental Sciences, University at Albany, State University of New York, Albany, New York.

Corresponding author: Robert G. Fovell, Department of Atmospheric and Environmental Sciences, University at Albany, State University of New York, Albany, NY, 12222, USA. Email: rfovell@albany.edu

9 ABSTRACT: We utilized high temporal resolution, near-surface observations of sustained winds
10 and gusts from two networks, the primarily airport-based Automated Surface Observing System
11 (ASOS) and the New York State Mesonet (NYSM), to evaluate forecasts from the operational
12 High-Resolution Rapid Refresh (HRRR) model, versions 3 and 4. Consistent with past studies,
13 we showed the model has a high degree of skill in reproducing the diurnal variation of network-
14 averaged wind speed of ASOS stations, but also revealed several areas where improvements could
15 be made. Forecasts were found to be underdispersive, deficient in both temporal and spatial
16 variability, with significant errors occurring during local nighttime hours in all regions and in
17 forested environments for all hours of the day. This explained why the model overpredicted the
18 network-averaged wind in the NYSM because much of that network's stations are in forested
19 areas. A simple gust parameterization was shown not only to have skill in predicting gusts in both
20 networks but also to mitigate systemic biases found in the sustained wind forecasts.

21 **SIGNIFICANCE STATEMENT:** Many users depend on forecasts from operational models and
22 need to know their strengths, weaknesses, and limitations. We examined generally high-quality
23 near-surface observations of sustained winds and gusts from the nationwide Automated Surface
24 Observing System (ASOS) and the New York State Mesonet (NYSM) and used them to evaluate
25 forecasts from the previous (Version 3) and current (Version 4) operational High-Resolution Rapid
26 Refresh (HRRR) model for a selected month. Evidence indicated that the wind forecasts are
27 excellent yet imperfect and areas for further improvement remain. In particular, we showed there
28 is a high degree of skill in representing the diurnal variation of sustained wind at ASOS stations
29 but insufficient spatial and temporal forecast variability and overprediction at night everywhere, in
30 forested areas at all times of day, and at NYSM sites in particular, which are more likely to be sited
31 in the forest. Gusts are subgrid even at the fine grid spacing of the HRRR (3 km) and thus must be
32 parameterized. Our simple gust algorithm corrected for some of these systemic biases, resulting
33 in very good predictions of the maximum hourly gust.

34 **1. Introduction**

35 Accurate wind forecasts are important in a number of areas, including and not limited to wind
36 energy (Piccardo and Solari 1998; Petersen et al. 1998), pollution transport (Arya 1999), and an-
37 ticipation and mitigation of damage resulting from strong winds (Holmes et al. 2014). An example
38 of the latter is the “Santa Ana” weather event (cf. Rolinski et al. 2019), a cool-season pattern
39 of offshore flow in Southern California that is known to dramatically increase the risk of large
40 wildfires (Westerling et al. 2004; Rolinski et al. 2016). Numerical modeling of Santa Ana events
41 using the Weather Research and Forecasting (WRF) model’s Advanced Research WRF (ARW)
42 core (Skamarock et al. 2019) for the purposes of model verification and wind reconstruction (e.g.,
43 Cao and Fovell 2016; Fovell and Cao 2017; Cao and Fovell 2018; Fovell and Gallagher 2018) has
44 revealed strengths and weaknesses of both the forecasts and the observations of the *sustained wind*,
45 which in practice implies averaging over periods of time such as 2 or 10 min. At mesoscale grid
46 spacings, short-period (e.g., 3-s) *gusts* are a subgrid-scale phenomenon, necessitating parameter-
47 ization in all operational numerical weather prediction models at this writing. There have been
48 many such parameterizations proposed (cf. Sheridan 2011), some being rather complex (Panofsky

49 et al. 1977; Nakamura et al. 1996; Brasseur 2001; Gray 2003; Stucki et al. 2016; Gutiérrez and
50 Fovell 2018; Benjamin et al. 2021, to name a few).

51 Many users rely on wind predictions from operational models such as NOAA's operational
52 High-Resolution Rapid Refresh (HRRR) (cf. Benjamin et al. 2016; Dowell and co authors 2022).
53 HRRR is based on WRF-ARW and has 3 km horizontal grid spacing covering the conterminous
54 United States (CONUS). A number of studies have focused on verification of HRRR forecast
55 fields, including wind speed (cf. Olson et al. 2019b; Pichugina et al. 2019; Wilczak et al. 2019). In
56 particular, Fovell and Gallagher (2020), hereafter FG20, presented a forecast verification of HRRR
57 version 3's (HRRRV3 or V3) 00 and 12 UTC cycles, which were selected for their relatively long
58 (36-h) forecast periods. (Although new HRRR cycles were launched hourly, only the 00 and 12
59 UTC model runs ran longer than 18 h in V3.) Also, while other select months were also examined,
60 the primary focus was on April 2019 as a representative time period.

61 In addition to the boundary layer analysis that employed high-resolution radiosonde data, an
62 evaluation of 2-m temperature and 10-m wind speed forecasts for \approx 800 Automated Surface
63 Observing System (ASOS) sites was conducted. These installations are typically, but not always,
64 found at airports. FG20 demonstrated that the HRRRV3 produced skillful forecasts when averaged
65 over the ASOS network although temperature biases were robustly related to station elevation
66 and wind biases were negatively correlated with observed speed. The latter means that “sites
67 characterized by slower observed winds were systematically more likely to be overpredicted while
68 windier sites were underestimated” (FG20), consistent with the results of prior studies focusing
69 specifically on Santa Ana events (cf. Cao and Fovell 2016; Fovell and Cao 2017; Cao and Fovell
70 2018; Fovell and Gallagher 2018).

71 In this work, FG20's evaluation of forecasts for ASOS stations was reconsidered from scratch
72 and considerably extended and improved. As in FG20, we started with April 2019, but the specific
73 emphasis is on hourly mean winds and maximum gusts with the discussion confined to the 00
74 UTC cycle in order to streamline the presentation. In this effort, data from the New York State
75 Mesonet (NYSM; Brotzge et al. 2020) were also analyzed and gust forecasts made using a simple
76 parameterization suggested by Cao and Fovell (2018, hereafter CF18) were considered. As version
77 4 of the HRRR (HRRRV4 or V4) became operational in December 2020, an analysis of April 2021
78 is also provided to highlight improvements and identify remaining challenges.

79 This work diagnoses systemic errors and weaknesses of a very skillful operational model for the
80 purposes of highlighting areas for potential future improvements. Another goal was to identify and
81 understand issues with available observational data. This paper is organized as follows. Section 2
82 describes the data and methods used in this study and Sections 3 and 4 present our analyses of April
83 2019 (HRRRV3) and April 2021 (HRRRV4), respectively, the latter emphasizing comparisons with
84 the Section 3 findings. Finally, Section 5 presents some conclusions and recommendations.

85 **2. Data and methods**

86 Anemometers of different types, including the sonic, cup and vane, and propeller varieties, are
87 used to sample the wind at some period we will term the sampling interval. These samples are then
88 averaged over a certain period, the averaging interval. The World Meteorological Organization
89 (WMO) standard (WMO 2018) specifies averaging intervals of 3-s and 10-min for the gust and
90 sustained (mean) wind, respectively. In a given report consisting of sustained wind (hereafter
91 usually termed simply as “wind”) and gust readings, the gust is conventionally the highest 3-s
92 value within the averaging interval used for the wind¹. The standard also specifies an anemometer
93 mounting height at 10 m above ground level (AGL) with adequate clearance around the instrument.
94 Ideally, the surrounding environment would consist of open flat terrain with obstacles no taller
95 than 4 m and more than thirty times their height (2° above the horizon) away from the anemometer
96 (WMO wind class 1). Adherence to these guidelines, however, is not all that common in practice.

97 NOAA makes HRRR model outputs available hourly and on the hour, providing forecasts of
98 10-m AGL wind speed representing an instant of time². However, because the winds at any grid
99 point only vary over time periods that are much longer than the model time step (20 s), these are
100 interpreted as sustained winds. As in FG20, 1-min ASOS observations were obtained from the
101 National Centers for Environmental Information (NCEI) archive, which are available for more than
102 850 sites in the CONUS. The 1-min observations provide measurements of sustained winds and
103 gusts made from sonic anemometers nominally at 10 m AGL. Although the internal processing
104 is complicated³, the sustained wind readings we used effectively represent an average of samples

¹In the United States, a significant exception to this is the Remote Automated Weather Station (RAWS) network, for which hourly reports consist of the past hour’s highest speed sample (peak wind) along with the mean wind of the last 10 min prior to the report (National Wildfire Coordinating Group 2019). Thus, there is no guarantee the peak came from the samples used to compute the sustained wind.

²The lowest horizontal wind model level is close to 10 m AGL and the 10-m wind speed value is obtained via vertical interpolation. See Benjamin et al. (2021).

³See documentation at <https://www.weather.gov/asos/>

105 taken over the 2-min period prior to the report, with the highest 3-s average during the 1-min
106 interval provided as the gust. The consequences of the relatively coarse (1 kt or 0.5144 m s^{-1})
107 precision of ASOS wind and gust reports will be noted in the analyses to come.

108 The FG20 analysis used top-of-the-hour ASOS reports and model fields were interpolated to
109 station locations in the usual fashion. However, owing to the model's horizontal resolution, which
110 does not resolve small turbulent eddies, there is very likely less temporal and spatial variability
111 in the forecasts than in the observations. To assess whether this unduly influenced the results,
112 we elected to pursue an alternative strategy in this new effort, using the observed *hourly mean*
113 *wind speed* and *hourly maximum gust*. Sustained wind observations from each site were averaged
114 through a 60-min window centered at the top of each hour and the largest gust report within that
115 window was identified. For each station, only hours without missing or invalid data in a given hour
116 were retained. Thus, we used hourly-averaged winds instead of 2-min averages in the sustained
117 wind verifications. Owing to Harper et al. (2010), who argued that different averaging intervals
118 represent “equivalent measures of the true mean wind but with differing variance”, we expected
119 that the results for the sustained wind would be nearly unchanged, and this proved to be true.

120 In contrast, the altered handling of the gusts did make a difference. In prior work using 1-min
121 ASOS observations (including Cao and Fovell 2016, 2018; Fovell and Gallagher 2018), the gust
122 in each station record represented the largest speed sample during the 1-min interval at the top of
123 each hour. Because this covers only 1.7% of the hour, we believe the hourly maximum gust is a
124 better measure of the wind threat. This caused a reasonable and anticipated change in the gust
125 factor (GF), being the gust divided by the sustained wind. Averaged over the CONUS, the 1-min
126 ASOS GF was about 1.29 and this increased to 1.86 with the new strategy. Further discussion may
127 be found in the Appendix.

128 Although most ASOS stations are at airports there are some significant exceptions, such as the
129 consistently windiest site (KDGP - Guadalupe Pass, TX), a non-airport installation sited near a
130 steep cliff. There are some very low wind speed stations, including non-airport sites such as
131 KMEH (Meacham, OR), KP69 (Lowell, ID), and KMHS (Mt. Shasta, CA), and small airports
132 possessing significant along-runway obstructions, examples being KVPC (Carterville, GA) and
133 K1JO (Bonifay, FL). A fraction of installations reportedly have anemometers mounted below 10

134 m AGL (e.g., KMTP - Montauk, NY). None of these problem stations were excluded from our
135 analyses because they were not found to alter our results or conclusions.

136 The New York State Mesonet (Brotzge et al. 2020) contains 126 surface stations distributed across
137 the state with an average spacing of 27 km. Each station possess sonic and propeller anemometers
138 mounted (apart from five rooftop installations in New York City) at 10 m AGL. Retention of these
139 rooftop sites did not change our results or conclusions. The precision of the sonic and propeller
140 anemometer readings are 0.1 and 0.17 m s^{-1} , respectively (G. Lufft Mess und Regeltechnik GmbH
141 2021; R.M. Young Company 2000). Quality controlled, three-second observations from both
142 sensors were obtained directly from the Mesonet. This would seem to represent an opportunity
143 to evaluate the influence of hardware on the wind measurements but there are some unfortunate
144 complications. The NYSM propeller instrument provided a 3-s average wind every 3 s, consistent
145 with the WMO gust standard and being the same gust averaging interval employed by the ASOS
146 sonic anemometers. In contrast, the NYSM's sonic instrument sampled once per second but only
147 every third reading was recorded, meaning its gusts are actually 1-s and not 3-s averages.

148 As with the ASOS data, we used the NYSM readings to construct hourly average winds and
149 hourly maximum gusts centered on the hour for both instruments, but retained only hours with
150 valid data from both instruments. Over April 2019 and 2021, mean propeller winds were about 0.25 m s^{-1}
151 (10.7%) lower than for the sonic, and gusts were 0.6 m s^{-1} (12%) slower, these differences
152 being large enough to be relevant to our analyses. The propeller anemometer reported relatively
153 more readings close to calm. The network-averaged GFs for April 2019 were 2.21 and 2.24 from
154 the propeller and sonic instruments, respectively. The shorter interval used with the sonic gust data
155 could be expected to increase the GF slightly (cf. Durst 1960).

156 FG20 did not consider gust forecasts. Herein we verified forecasts made using the simple CF18
157 parameterization for 10-m gusts, which consisted of multiplying the (sustained) wind forecast by
158 the network-averaged GF after correcting for the mean network-averaged bias. We note the HRRR
159 model also provides “gust potential” forecasts created using boundary layer depths and winds
160 (Benjamin et al. 2021). However, in the hourly HRRR outputs, these forecasts are instantaneous
161 values. It would be inappropriate to consider them as predictions of the hourly maximum gust
162 and they do not verify well against them anyway (not shown). The HRRR makes subhourly (every
163 15-min) forecasts available, but these neither fully sample the hour nor are available beyond forecast

164 hour 18, even in HRRRV4. As a consequence, we did not consider the HRRR's gust forecasts in
165 this study.

166 **3. HRRRV3 wind and gust evaluation for April 2019**

167 Figures 1 and 2a show the topography and primary landuse assignments used by the HRRRV3.
168 Landuse and terrain information was obtained from the WRF Geogrid file made available on
169 NOAA's HRRR website (<http://rapidrefresh.noaa.gov/hrrr/>). In WRF-ARW version 3, on which
170 HRRRV3 was based, there were two separate landuse databases derived from MODIS (Moderate
171 Resolution Imaging Spectroradiometer) satellite information available with HRRRV3 employing
172 the lower-resolution version. Surface roughness lengths (z_0), constructed as described in He et al.
173 (2021), were extracted from model outputs at forecast hour 12⁴.

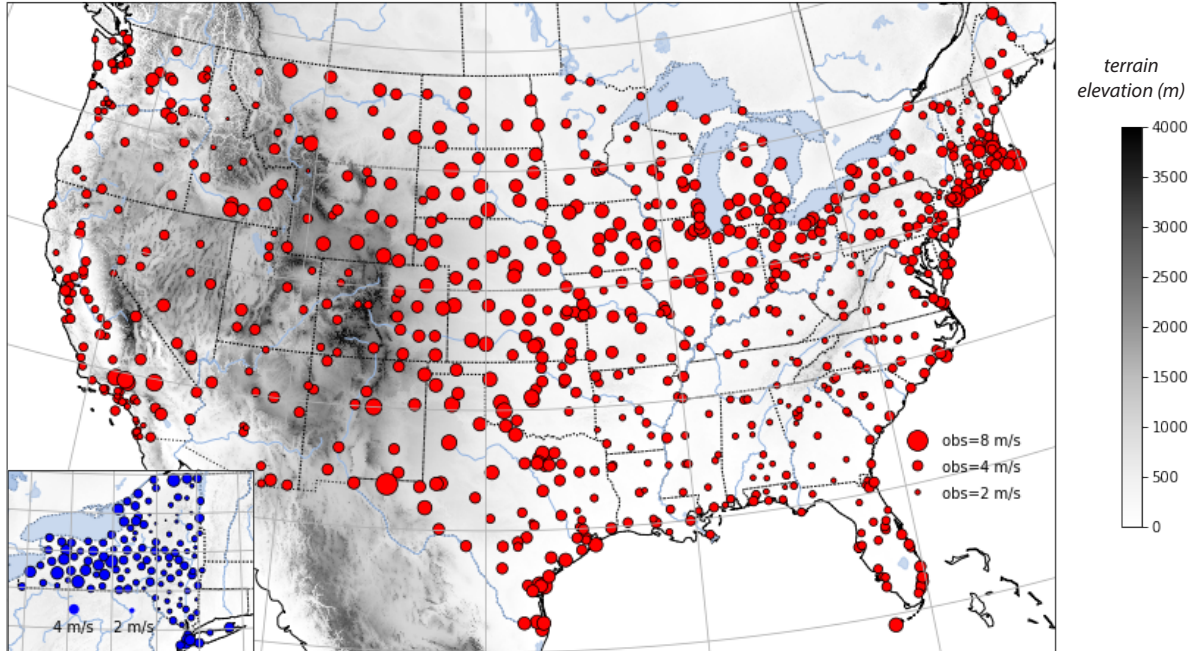
174 The locations of 807 ASOS and 126 NYSM sites are also shown on Fig. 1, with marker size
175 reflecting mean wind speed for April 2019. Sites with fewer than 500 observations in the month
176 were excluded from the analysis and are not shown. Owing to finite resolution, a few stations were
177 misclassified as being over water (including having $z_0 < 0.01$ m), and these were also removed.
178 WRF-ARW and the HRRR's Rapid Update Cycle (RUC) land surface model utilize fractional
179 landuse assignments, and more than half (53%) of the ASOS stations were associated with more
180 than one class (Fig. 2b). This can and does influence surface characteristics (including roughness)
181 used in a given grid cell. That being said, the class representing the primary assignment had
182 an average landuse fraction of 0.84 over the 807 ASOS sites, this ranging from 0.74 among the
183 forested lands to 0.88 for the cropland and urban classes.

192 *a. Analysis by forecast hour and local time*

193 As in FG20, we first considered ASOS network-averaged winds expressed in terms of forecast
194 hour, which extended out to 36 h for the 00 UTC cycle. The present result (Fig. 3a) is nearly
195 identical to that shown in FG20 (their Fig. 7a), illustrating that the adoption of hourly mean
196 observations made essentially no difference. Again, the model started with a small negative bias
197 (defined as forecast minus observation) of about -0.5 m s^{-1} that became smaller in magnitude with
198 time over the first 24 forecast hours. This bias is small compared to the spatial variation of the

⁴In WRF-ARW, roughness lengths reported in the 0 h model output has not yet been updated, and thus may not be correct.

HRRRV3 terrain map and April 2019 mean wind speeds

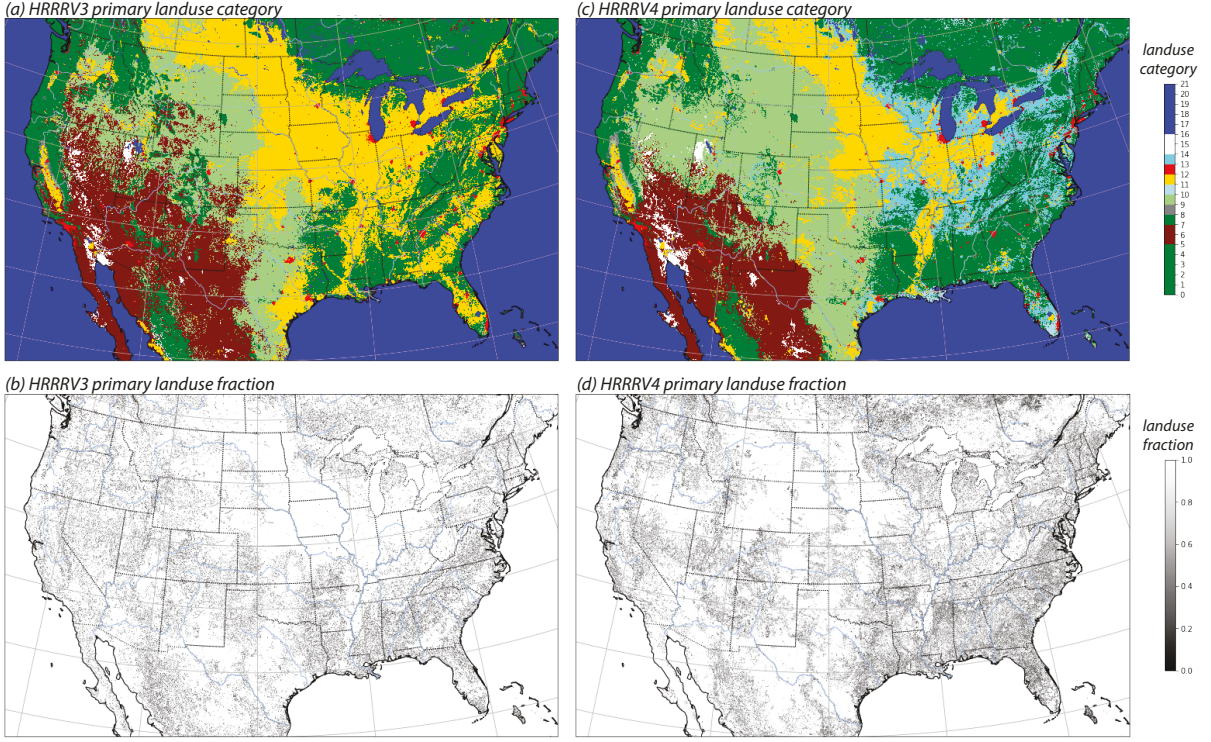


184 FIG. 1. Topography of the HRRRV3 domain, superposed with locations of 807 ASOS stations (red) and 126
185 NYSM sites (blue, in inset) retained in the April 2019 analysis. Marker sizes indicate monthly average wind
186 speed from April 2019, using observations from all times of day.

199 observations (illustrated by the grey vertical bars) owing to fact we are averaging across a very
200 wide area spanning four time zones.

201 New to this evaluation are examinations of forecast and observation spatial and temporal variabil-
202 ity and an analysis by local time (LT). Figure 4a reveals that the spatial variation of the forecasts
203 valid at ASOS sites (henceforth, “ASOS forecasts”), expressed as the standard deviation, was
204 smaller than that of the observations at all forecast hours. There is a diurnal cycle in both, again
205 smeared by averaging across time zones. This may be in part a consequence of local landscape
206 features (valleys, hills, obstacles and/or land surface variations) that cannot be resolved in the
207 model. Since the *mean* forecast and observed winds were quite similar, it can be anticipated that
208 the model would fail to represent the frequency of both lower and higher wind speeds. This will be
209 examined presently. Additionally, Fig. 4b presents time series of the difference between forecast

HRRRV3 and HRRRV4 landuse maps



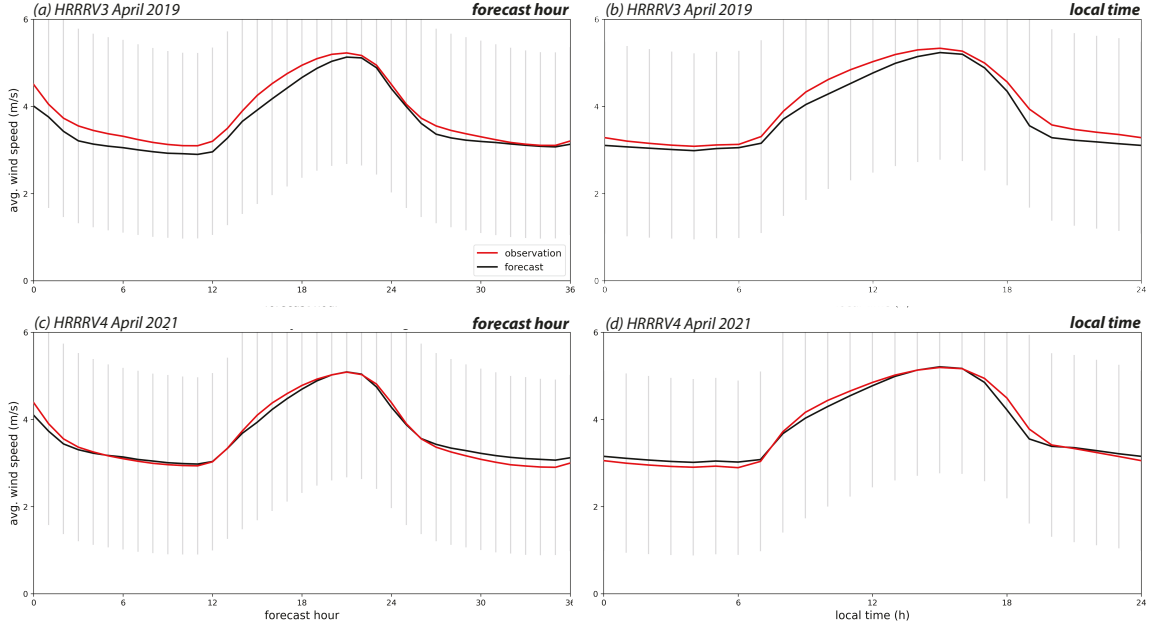
187 FIG. 2. Primary landuse assignments used in the (a) HRRRV3, and (c) HRRRV4, color coded by landuse
 188 category, showing ocean and lakes (blue), croplands (gold), grasslands (light green), evergreen, deciduous, and
 189 mixed forests and woody savannas (dark green), open shrublands (maroon), and urban (bright red) and barren
 190 (white) lands. In (b) and (d), fraction (0-1) of the primary landuse classification in the HRRRV3 and HRRRV4,
 191 respectively.

210 and observation spatial standard deviation and the forecast wind bias. They are similar in that they
 211 both were negative but became less so with time.

220 Expressed in terms of LT, the network-averaged forecasts retained a negative bias through
 221 the day (Fig. 3b), with the model apparently ramping up the late morning winds too slowly
 222 and diminishing them too quickly into the evening⁵. The HRRR model employs the Mel-
 223 lor–Yamada–Nakanishi–Niino Level 2.5 (MYNN2) planetary boundary and surface layer param-
 224 eterizations (Nakanishi and Niino 2004) which have been refined in recent years (cf. Olson et al.
 225 2019a). This finding may hold clues for further parameterization improvements. There was a

⁵The analysis time, forecast hour 0, was removed from this analysis owing to the shift in bias behavior seen between the analysis and forecast hour 1 in Figs. 4a and b.

HRRR 00Z cycle ASOS network-averaged 10-m wind by forecast hour and local time: April 2019 and 2021

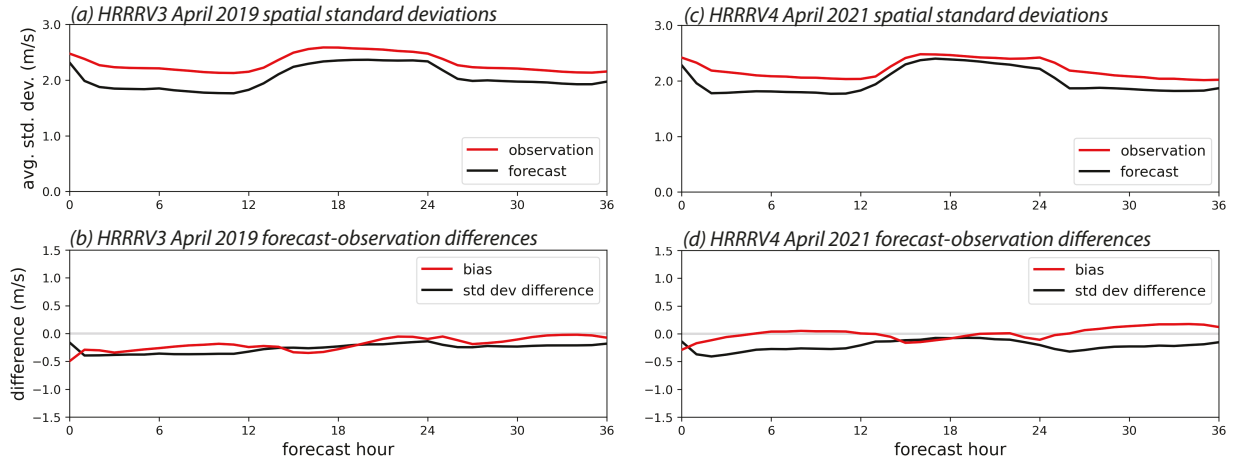


212 FIG. 3. Time series of ASOS observations (red) and HRRR forecasts (black) of 10-m sustained wind speeds,
 213 averaged spatially across the ASOS network and temporally over the month of (a, b) April 2019, and (c, d) April
 214 2021, presented with respect to HRRR forecast hour (left) and local time (right). On all plots, the vertical grey
 215 bars denote ± 1 standard deviation of the averaged observations.

226 diurnal cycle in both forecast and observation spatial variation (Fig. 5a) but again the forecast vari-
 227 ability was slightly smaller and the diurnal variation in spatial standard deviation difference and
 228 forecast bias was very small (Fig. 5b). It is emphasized that this is an excellent, if not completely
 229 perfect, forecast, at least with respect to the network average.

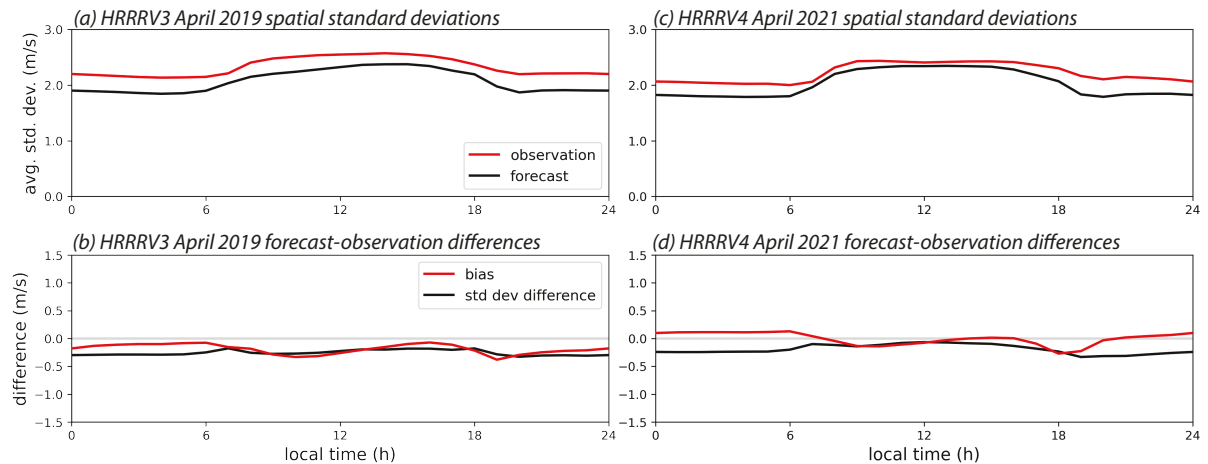
230 In pointed contrast, the HRRRV3 overpredicted wind speeds averaged over the 126 NYSM sites
 231 by more than 1 m s^{-1} (Fig. 6a). Part of this gap is due to the propeller instrument that, as noted
 232 above, reports lower sustained wind speeds than its sonic counterpart. However, the forecast bias
 233 with respect to the sonic observations was 0.77 m s^{-1} , which is still sizable. Another difference
 234 is that the spatial variability of the forecasts (Fig. 6b) was larger than the observations at every
 235 forecast hour with the biases and spatial standard deviation differences being relatively constant
 236 with forecast hour (Fig. 6c). We need to emphasize at this point that the ASOS and NYSM networks

HRRR 00Z cycle ASOS network averages by forecast hour: April 2019 and 2021



216 FIG. 4. Time series of the spatial standard deviation of ASOS observations (red) and HRRR forecasts (black)
217 of 10-m wind speed for April 2019 and April 2021 (top row), and of forecast minus observation average wind
218 speed (bias, red) and spatial standard deviation (black) for these same two months (bottom row). All are shown
219 with respect to HRRR forecast hour.

HRRR 00Z cycle ASOS network averages by local time: April 2019 and 2021



216 FIG. 5. Similar to Fig. 4 but expressed in terms of local time.

217 serve different needs and represent markedly different siting philosophies. Instead of being largely
218 colocated with airports, NYSM stations sample the landscapes and geography of the state.

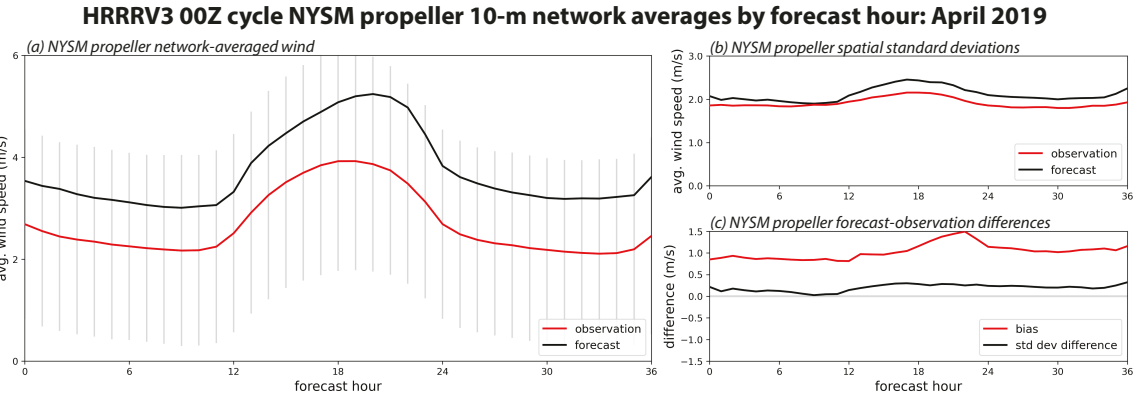


FIG. 6. Similar to Figs. 3a and 5a,b but for the NYSM propeller observations and forecasts.

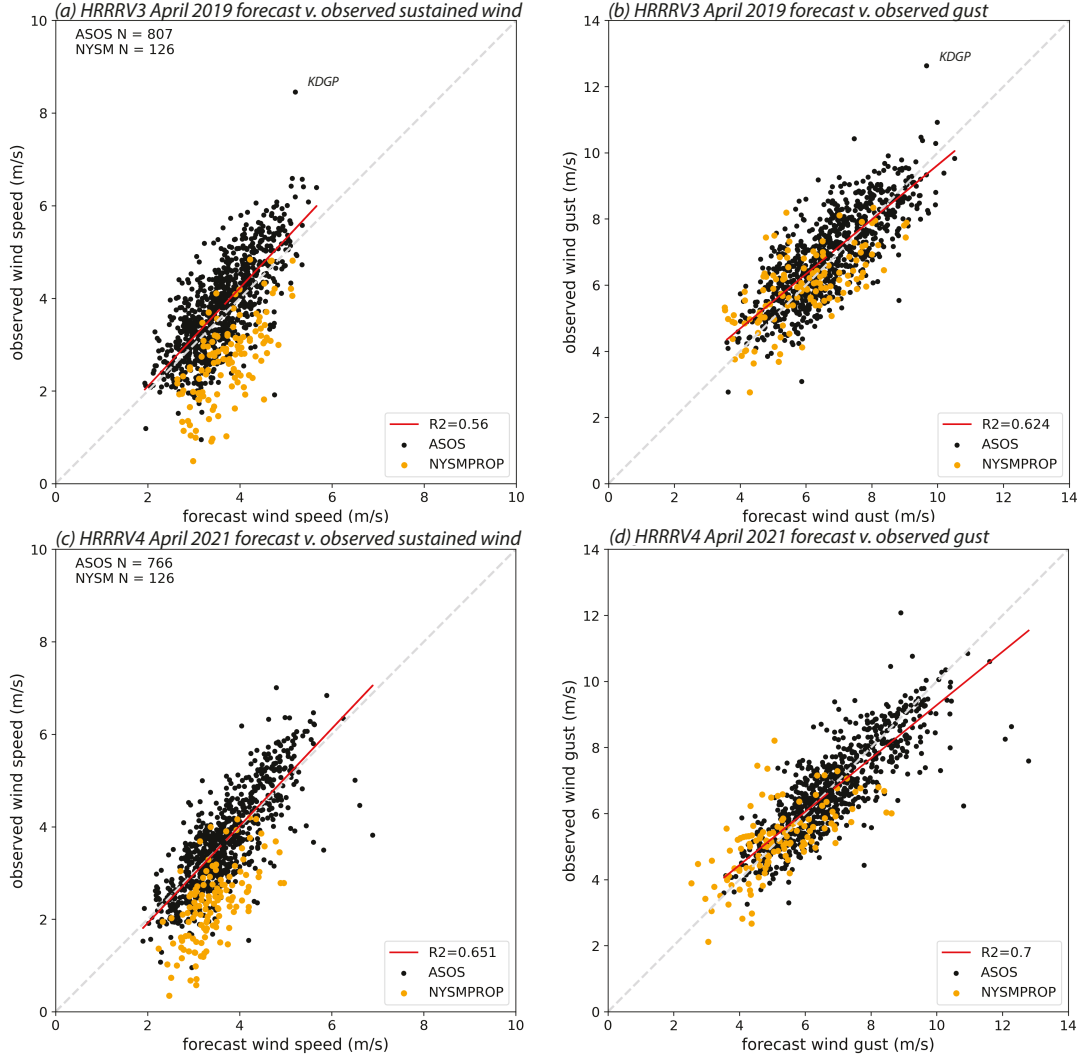
239 *b. Analysis by station*

240 The present study also enhanced the station-based analysis of FG20 and the previously cited work
 241 on Santa Ana winds. We started by comparing forecast and observed sustained winds averaged
 242 over all available pairs for each station (Fig. 7a). Each dot is an ASOS (black) or NYSM (orange)
 243 station. Regarding the ASOS sites, while there are a few, non-impactful outliers, the squared linear
 244 correlation coefficient between the series is moderately high ($R^2 = 0.56$) and largely arrayed along
 245 the 1:1 correspondence line. NYSM stations are generally found beneath the 1:1 line, consistent
 246 with the overprediction already demonstrated. The least-squares fit shown was based solely on the
 247 807 ASOS sites.

248 The relationship between forecast wind bias and various variables is examined in Fig. 8. Similar
 249 to previous studies already cited, the forecasts were not correlated with the bias (Fig. 8a), even
 250 for NYSM stations (orange circles). However, the observations were significantly and negatively
 251 correlated with bias (Fig. 8b), indicating overprediction of calmer sites and underprediction at
 252 windier locations. The NYSM stations do not appear to be exceptional, apart from the fact that
 253 as a relatively low wind speed network their sites are more likely to be associated with positive
 254 biases. A comparable analysis using the NYSM's sonic observations was only subtly different (not
 255 shown).

256 CF18 demonstrated (their Fig. 11d) that the forecast wind bias was also positively correlated
 257 with the station gust factor, which could be expected because GF incorporates the observed wind.
 258 They used station GF *relative to the network average value* to interpret the forecast bias and infer

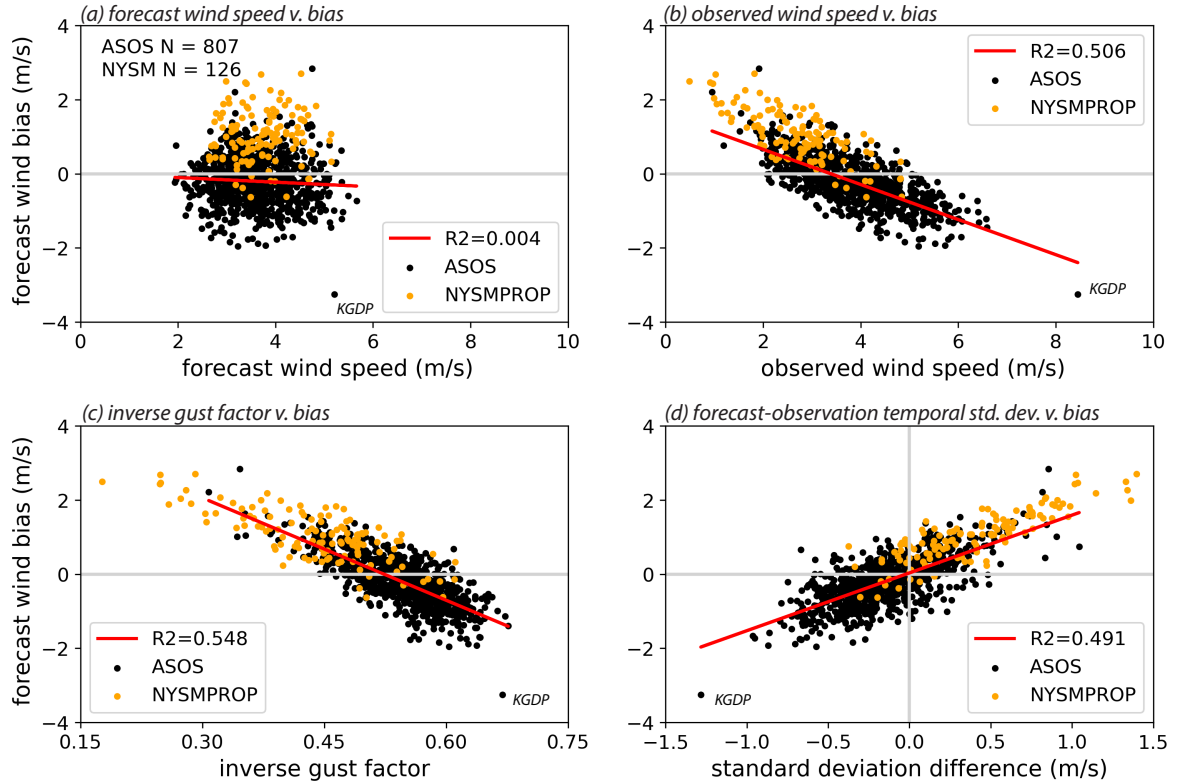
HRRR 00Z cycle ASOS station analysis: April 2019 and 2021



256 FIG. 7. Forecast vs. observed (a) wind and (b) and gust speeds averaged over all forecast/observation pairs
 257 from April 2019 or April 2021, aggregated by station. Here each dot is an individual station, either ASOS (black)
 258 or NYSM propeller (orange). Gust forecasts used the CF18 strategy (see text). Least squares fits (red lines)
 259 are based only on ASOS sites. Panels (c) and (d) are for April 2021. For April 2019, ASOS station KDGP is
 260 identified. This station had insufficient observations for April 2021.

268 site exposure. Locations with significant obstructions would be expected to have relatively lower
 269 wind speeds than similar although unobstructed sites, but short-period gusts might be anticipated
 270 to be less impacted, leading to higher GF values. Wind speeds at these stations would be expected
 271 to be overforecast because the model cannot “see” and account for these obstructions. In contrast,

HRRRV3 00Z cycle ASOS/NYSMPROP forecast wind bias station analysis: April 2019



261 FIG. 8. Station averages from April 2019 of (a) forecast wind speed, (b) observed wind speed (c), inverse gust
 262 factor, and (d) temporal standard deviation difference (forecast-observation) presented vs. station average forecast
 263 wind bias for ASOS (black) and NYSM (orange) stations. Least squares fits (red lines) shown only incorporated
 264 ASOS sites. ASOS station KDGP is identified.

262 sites with lower GFs might have local features, such as hills, that might help speed up the wind
 263 relative to a more average setting. These stations would likely be underpredicted.

264 In Fig. 8c, we see a sizable negative correlation between bias and GF, although here we have
 265 instead elected to employ its reciprocal, the inverse gust factor (iGF), because it improves the
 266 linear relationship with bias and is bounded between 0 and 1. GF and iGF are functions of the
 267 observational data only and we see the model tended to overpredict when the sustained wind speeds
 268 were particularly small relative to the gust and underpredict when they were more comparable.

269 CF18 also considered a simple gust parameterization that was inspired by the association between
 270 bias and GF (and thus iGF). That strategy partially compensated for the biases in the sustained

wind forecasts by applying the network-average gust factor to *all* wind forecasts, yielding less biased gust predictions. Underpredicted stations also tended to have smaller GF (larger iGF) values than average, so multiplying the too-low speed forecasts by the network average at least partially mitigated the model’s negative sustained wind bias. Similarly, overpredicted sites often had larger than average GFs (smaller iGFs) so multiplying the positively biased forecasts by the smaller network-average GF compensated for some of the overprediction.

This idea was applied to the April 2019 HRRR forecasts and is shown in Fig. 7b. In this case, ASOS wind forecasts were multiplied by 1.86, being roughly the network’s average GF for the hourly maximum gust. This GF was applied to forecasts made for the top of the hour because we have insufficient information to determine the hourly mean forecast wind speed. With that caveat, we note this very simple gust parameterization performed quite well, with an even higher R^2 (0.62) than the forecast/observed wind relationship. Again there is a tendency for forecast/observation pairs to spread along the 1:1 line.

The CF18 parameterization implicitly presumed the network-averaged forecast wind bias was negligible so application of a single GF value could mitigate errors relative to the average. That is not the case for the NYSM. Figure 7b also shows (again in orange) NYSM gust forecasts made using that network’s average GF (2.21), after adjustment for the mean forecast wind bias of about 1 m s^{-1} . Compared to the sustained winds, these gust forecast/observation pairs clustered much closer to the 1:1 line.

Finally, Fig. 8d demonstrates that the difference between forecast and observation temporal standard deviation was also well-correlated with forecast bias. Note now the standard deviations represent the *temporal* variability of the forecasts and observations at each station. Stations at which the forecasts have more variability than the observations tended to be overpredicted with respect to wind speed and underprediction often resulted at stations where the observations had more variation. However, as with GF and iGF, this variable is not independent of the observed wind. The standard deviation of a variable like wind speed, which has the hard constraint of being non-negative, can (and, although not shown, generally does) increase with the variable magnitude.

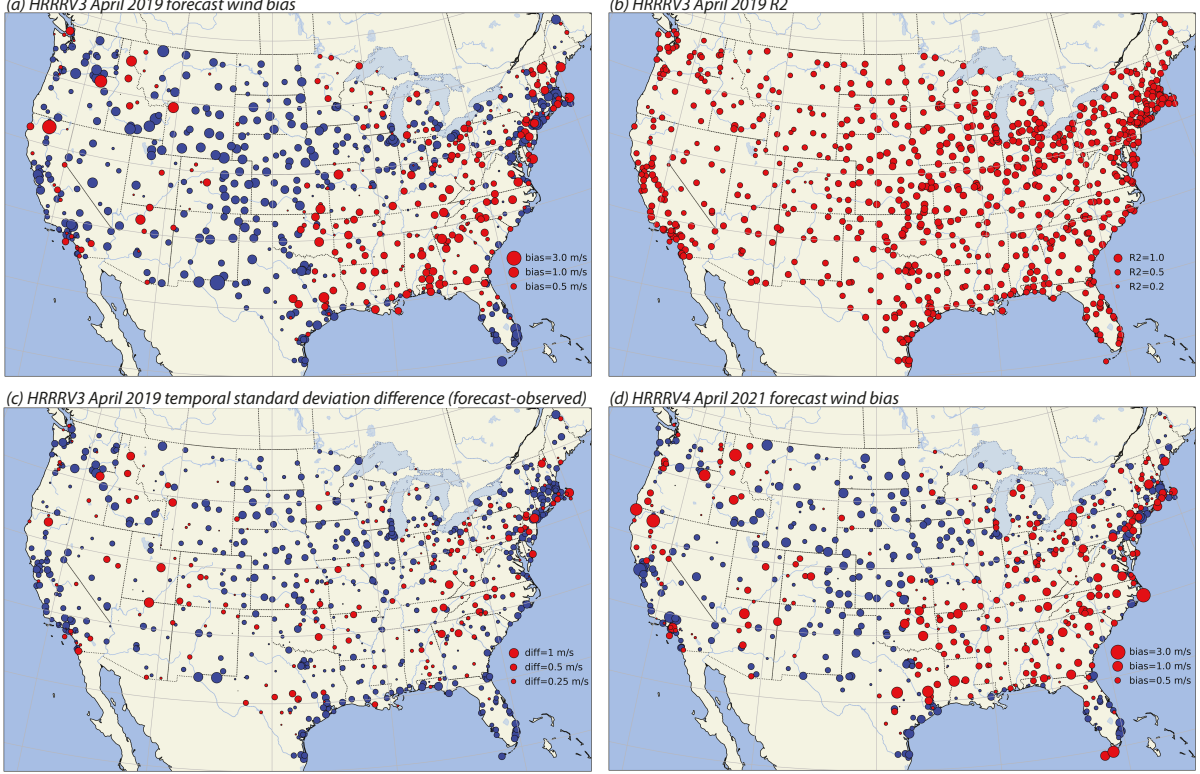
Spatial plots (Fig. 9) were examined to look for patterns. While the average forecast wind bias, computed over all stations and forecast hours, was only -0.2 m s^{-1} (cf. Fig. 3a), it remains that 507 of the 807 stations (63%) were underpredicted in the mean. Figure 9a shows that the

311 positively biased stations were concentrated in the Southeast, the Appalachians generally, and into
312 the Northeast where forested land is more common (Fig. 2a). In Fig. 9b, marker size reflects
313 the squared linear correlation between the forecast and observed winds, based on an average of
314 1000+ forecast/observation pairs from each site. R^2 values ranged between 0.03 (KP69) and 0.77
315 (KARR - Aurora, IL) with a mean of 0.57 and median of 0.59. Correlations were high throughout
316 most of the country, even in the Southeast where mean winds were relatively light, and lowest
317 in the mountainous West. Like the correlation coefficient, R^2 is not sensitive to means or mean
318 differences between series and is most likely low where the predictions are somewhat out of phase
319 with the measurements. The concentration of low correlations in the western CONUS may reflect
320 the influence of local features on diurnal winds that the model fails to properly represent.

321 Figure 9c reveals how the temporal standard deviation difference between the forecasts and ob-
322 servations varied spatially. Figure 8d showed that the former tended to be the larger when observed
323 wind speeds were low and forecasts were positively biased. The mean and median differences were
324 -0.15 and -0.17 m s^{-1} , respectively, with 581 (72%) of the sites having less variability among the
325 forecasts than the observations. Note that the large red dots (representing larger forecast than ob-
326 servation variability) are few in number and widely scattered. These are stations having significant
327 local obstructions near the ASOS installations. For those sites, observation variability was likely
328 suppressed by limited anemometer exposure. This measure could be used to identify problem sites
329 for potential removal from analyses and data assimilations.

333 Taken together, this analysis suggests that the small negative forecast bias seen in the network
334 averaged winds (Fig. 3) is more significant than it might appear at first glance. The majority
335 of locations have insufficient forecast variability that is strongly correlated with negative biases.
336 This suggests the model is not capturing something that is important to determining real winds
337 measured in the field. However, this is partly compensated by the inclusion of stations that are not
338 at airports and/or have obvious siting issues. Had those sites been removed from the analysis, the
339 underprediction would have been more pronounced. The model is still very skillful but steps could
340 be taken to address its tendency to underestimate the mean winds at better exposed locations.

HRRRV3 and HRRRV4 station analysis maps: April 2019 and 2021



330 FIG. 9. Spatial plots of (a) average forecast wind bias, (b) forecast-observation squared correlation R^2 , and
 331 (c) temporal standard deviation difference (forecast-observed) for April 2019. Panel (d) shows average forecast
 332 wind bias for April 2021. For (a), (c), (d) positive values are red, negative are blue.

341 *c. Analysis of forecast/observation pairs*

342 In their analysis, FG20 examined scatterplots involving all individual ASOS forecast and obser-
 343 vation pairs over a full month and this provided insight into the source of forecast biases. Here,
 344 we improve and extend that analysis, examining all 827,230 April 2019 pairs⁶. This represents the
 345 concatenation of forecasts and observations from 807 ASOS stations and all forecast hours from
 346 the daily 36-h HRRRV3 00 UTC cycle forecasts. Note that many observations were paired with
 347 more than one forecast.

348 All ASOS forecast/observation pairs are presented as a heatmap, color coded by point density,
 349 in Fig. 10a. Although there is scatter about the 1:1 correspondence line, there is a reasonably good

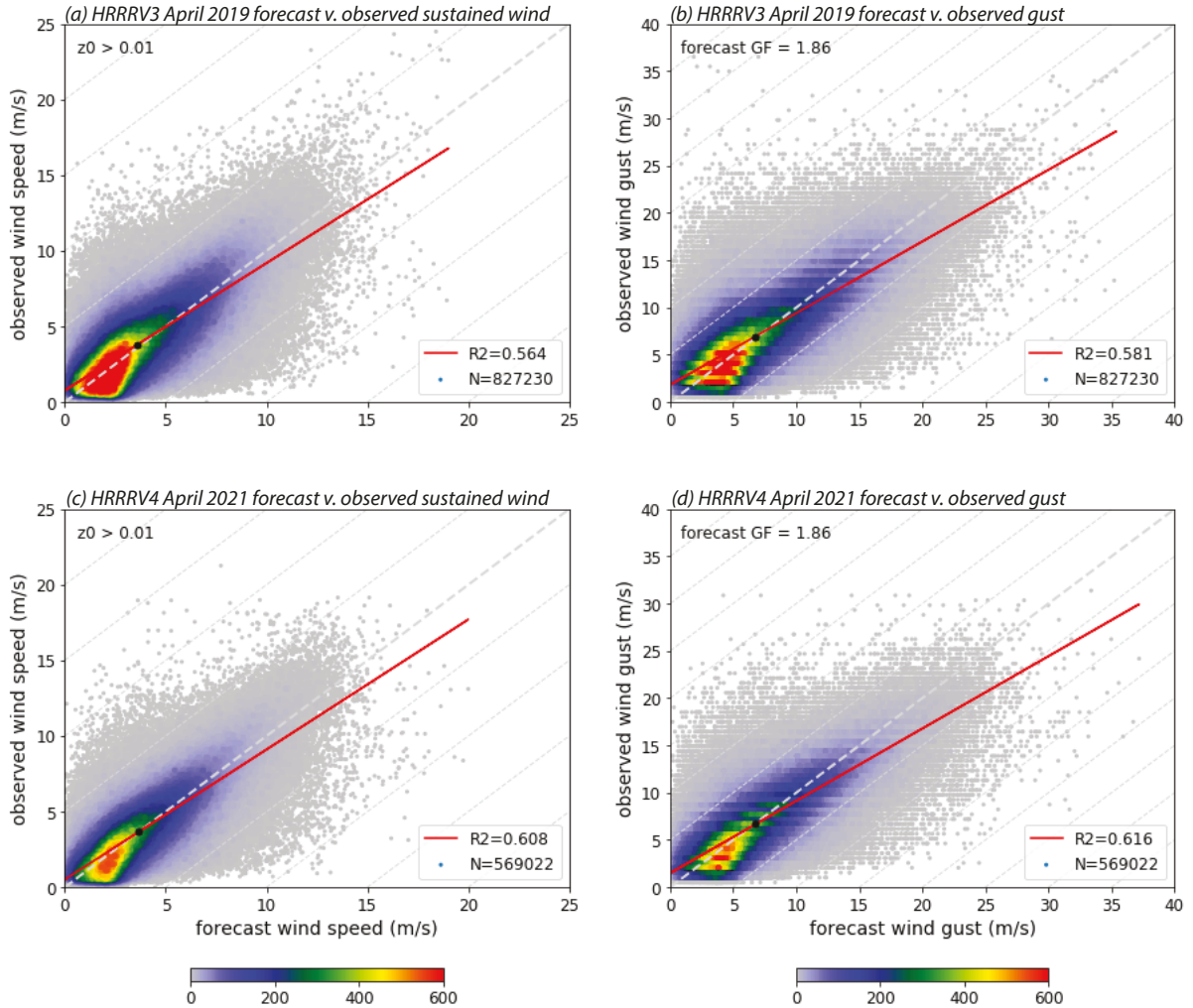
⁶There are fewer pairs in the present analysis than in FG20 (851,550) owing to the more stringent restrictions employed in the construction of hourly-averaged observations.

350 relationship ($R^2 = 0.56$) between these variables, comparable to that seen in the station-averaged
351 analysis (Fig. 7a). The majority of observations and forecasts represented speeds less than 5 m s^{-1} ,
352 and this fact drives the relationship. For higher observed winds, however, the forecasts still largely
353 spread along the 1:1 line, indicating some usable skill. Similarly, all forecast gusts – created via
354 the constant GF of 1.86 – are plotted against observed gusts in Fig. 10b. As was the case with the
355 station-averaged analysis, the correlation is higher for the gust forecasts than their sustained wind
356 counterparts.

362 However, these same data viewed as histograms (Fig. 11) demonstrate that the forecast and
363 observed wind and gust distributions had distinctly different shapes. The forecasts possessed a
364 narrower peak such that the occurrence of both lower and higher observed winds was relatively
365 more frequent. This result was suspected in the discussion of Fig. 4a above. Motivated by Fig. 8c,
366 we also examined histograms of winds and gusts partitioned into lower and higher GF segments
367 (Fig. 12). Forecast and observation pairs were separated into two groups based on the GF associated
368 with the observation relative to the median value (about 1.81). With respect to winds (panels a, b)
369 there is a much larger shift between the segments in the shapes of the observed wind distributions
370 than for the forecasts. When the GF is lower, the observed distribution is shifted rightward, resulting
371 in more observations than forecasts of values exceeding 3.5 m s^{-1} . In contrast, observations in the
372 high GF half are skewed towards lower speeds, resulting in a mean positive bias.

377 To reiterate, the network mean bias of ASOS forecasts was nearly zero (Fig. 3a,b), but the bias
378 was biased such that stations having lower average wind speeds were overpredicted while windier
379 ones were underforecast (Figs. 8c, 11a). The constant GF algorithm exploits this systemic tendency
380 to underpredict at sites where GFs lower than the network average and overpredict at the others by
381 multiplying these biased wind forecasts by a single number (the network average GF), the result
382 being *less biased gust forecasts* (Fig. 12c,d). For locations in space and/or instances in time where
383 the observed GF was lower than the network average, multiplying by the larger average value helped
384 shift the forecast gusts more into alignment with the observations (Fig. 12c). Similarly, multiplying
385 forecasts of high GF instances or locations by the smaller network average helped correct for the
386 deficiencies seen among the sustained winds. The result is not perfect and we have already seen
387 that when the two segments are recombined (i.e., Fig. 11a), the forecast range is too narrow relative

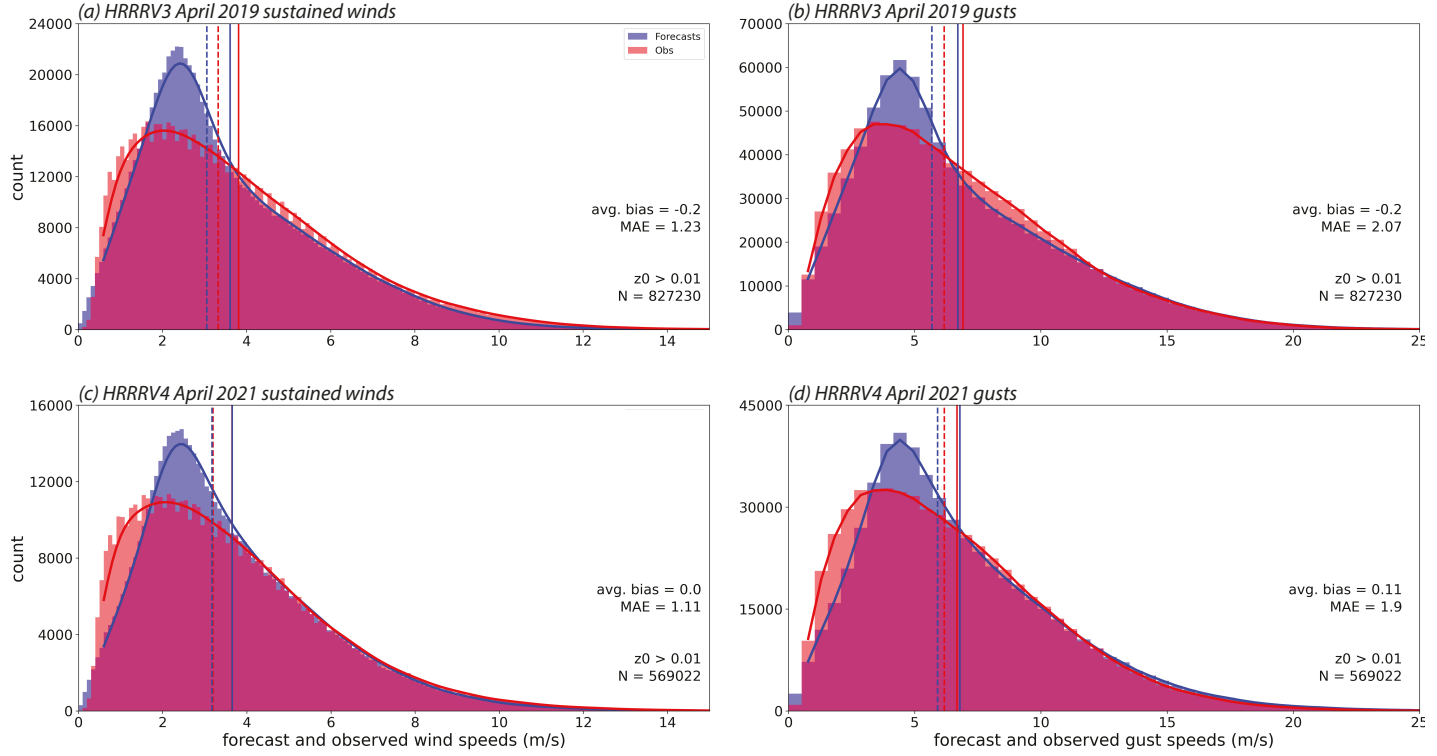
HRRR 00Z cycle ASOS pairwise analysis: April 2019 and 2021



357 FIG. 10. All forecast/observation pairs of wind speed (left) and gust (right) for ASOS stations during April
 358 2019 (top) and April 2021 (bottom). Color shading indicates point density and the linear regression line for each
 359 is shown in red. Gust forecasts were produced using the ASOS network average GF. The black dot is the joint
 360 mean. $z_0 > 0.01$ indicates that sites misclassified as being over water have been removed. This is true for all
 361 analyses in this study.

388 to the observations. In the next section, we will discover reasons for the excessive sharpness in the
 389 forecast distributions.

HRRR 00Z cycle ASOS histograms: April 2019 and 2021

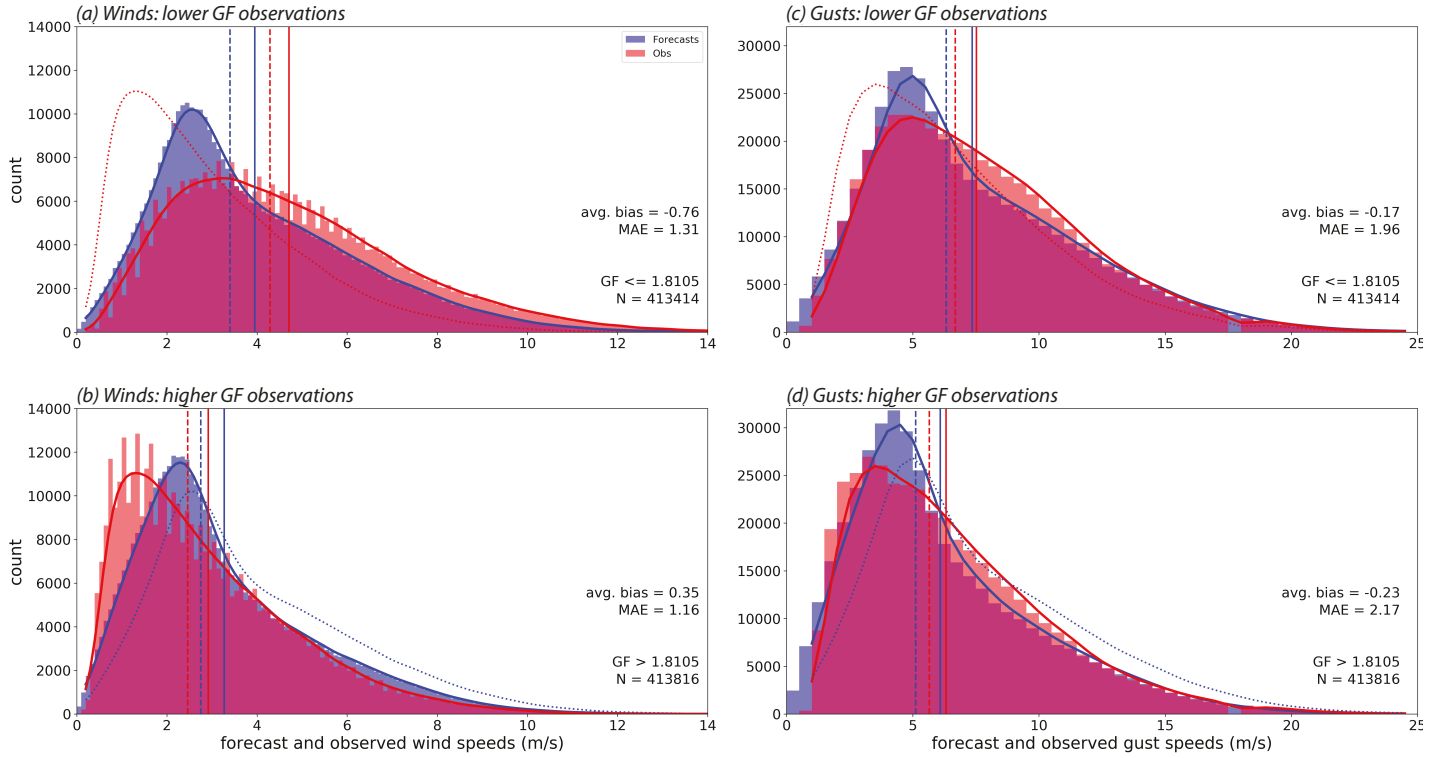


373 FIG. 11. Histograms of all forecast (blue) and observed (red) wind speeds (left) and gusts (right) for April
 374 2019 (top) and April 2021 (bottom). MAE stands for mean absolute error. Vertical solid lines indicate mean
 375 values and dashed lines represent median values. A wider bin size was used for gusts owing to the coarse (1 kt)
 376 precision of hourly maximum gust observations.

394 *d. The roles of landuse and local time*

395 The potential roles of landuse type and local time were investigated to understand the differences
 396 between the observations and forecasts, especially with respect to their distributional shapes as
 397 seen in Fig. 11. As noted earlier, WRF-ARW uses fractional landuse allocations (cf. Fig. 2b) and
 398 the focus here is on the largest, or primary, assignment. For HRRRV3 and April 2019, 41% of
 399 the ASOS stations had a primary classification of cropland, 24% were urban, 14% had grassland,
 400 and 6% were given open shrubland assignments. The various forested land classes, including
 401 deciduous, evergreen, and mixed forests, accounted for about 11% of the ASOS sites. While
 402 unsurprising, it is clear that the urban landuse type is substantially overrepresented in the ASOS
 403 network relative to the CONUS landscape (see, for example, the bright red areas in Figs. 2a,c).

HRREV3 00Z cycle ASOS histograms by gust factor: April 2019



390 FIG. 12. Similar to Fig. 11a,b but showing the April 2019 wind and gust distributions subdivided at the median
 391 GF (about 1.81). The dotted red curves in (a) and (c) represent the higher GF observation distributions, to facilitate
 392 comparison. Similarly, the dotted blue curves in (b) and (d) represent the lower GF forecast distributions. The
 393 sawtooth variation in the observations in (a) and (b) is another consequence of the gust data precision.

404 Figure 13 reveals the existence of a robust association between primary assignment and forecast
 405 wind bias. Each class possesses two horizontal bars, representing the average bias (blue, units m s^{-1}) among stations with that classification and their weighted contribution (red, units dm s^{-1} for
 406 convenience) reflecting station count towards the network-average bias of -0.2 m s^{-1} . The most
 407 negative bias (-0.6 m s^{-1}) was associated with the open shrublands stations but the urban and
 408 grassland sites had larger weighted shares owing to their larger station counts. Similarly, although
 409 cropland stations had a small class-average bias (-0.08 m s^{-1}), their aggregate effect was not minor
 410 owing to their ubiquity (41% of stations). In contrast, the roughly 11% of installations residing in
 411 forested grid cells were positively biased, by as much as $+0.52 \text{ m s}^{-1}$ in the evergreen needleleaf
 412 forest.

413 cells⁷. If these overpredictions were resolved in isolation, the network-averaged skill would actually
414 *decrease*.

420 Figure 14 presents histograms of forecast and observed sustained wind similar to Fig. 11a but
421 have been segregated by selected primary landuse classes. All of the forecast distributions are
422 too sharp and narrow relative to the observations. In urban areas (panel a), the observed wind
423 distribution has spread farther to the right, revealing underforecasts of speeds exceeding about 3.5
424 m s^{-1} . That tendency was even more pronounced in the grassland and open shrubland group (panel
425 b), which have been combined owing to their similarity. The small negative bias in the cropland
426 class (panel c) occurred despite general overprediction of winds weaker than 1.5 m s^{-1} .

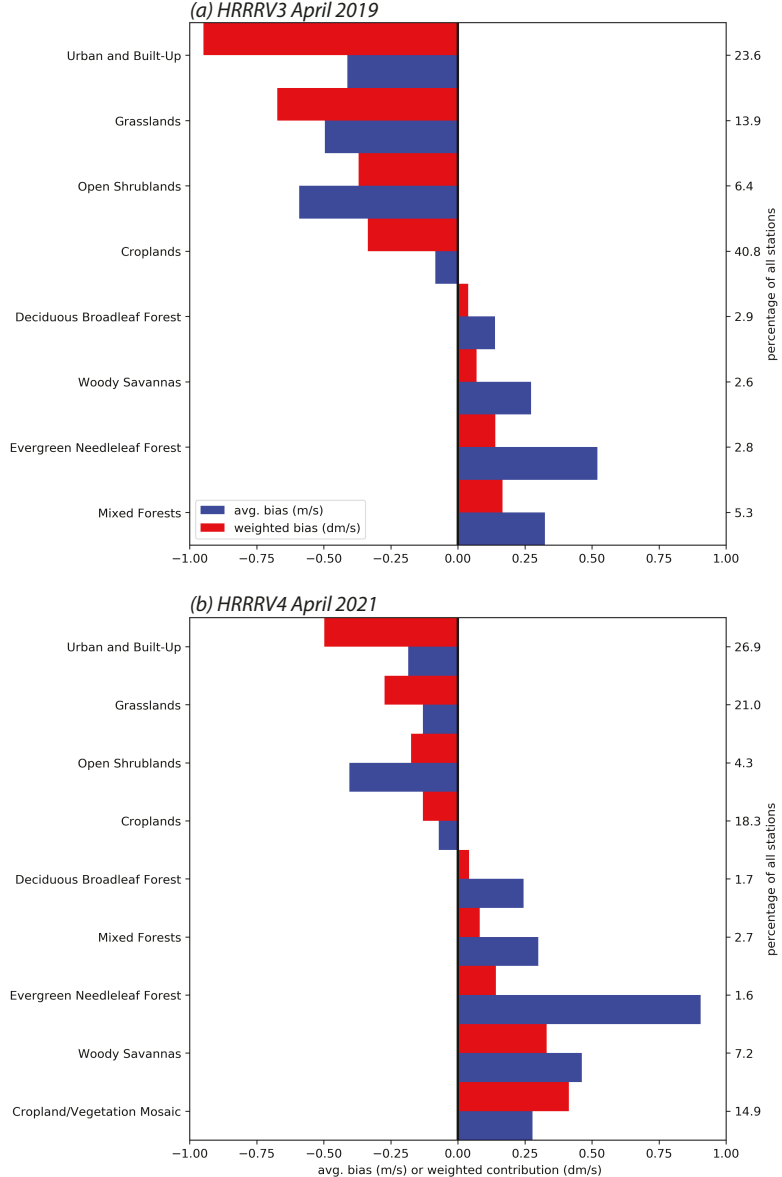
430 Importantly, the model has obviously failed to properly represent the general slowness of the
431 winds in the forested areas (Fig. 14d). This elucidates why the network-averaged sustained winds
432 from the NYSM were so overpredicted. Note that the Mesonet's sustained wind histograms
433 (Fig. 15) bear a strong resemblance to that of the ASOS forested class, independent of anenometer
434 type. While only 11% of the ASOS sites were classified as forested in the HRRRV3, that category
435 represented 43% of the Mesonet stations, and thus it exerts a powerful influence on this network's
436 average. Landuse type can affect wind forecasts through the roughness length, z_0 . Although this
437 would require testing, it is not clear that simply raising z_0 would improve these predictions because
438 the more serious issue is site exposure.

441 When the day is subdivided into four 6-hour segments as in Fig. 16, we clearly see the under-
442 prediction of observed ASOS winds exceeding 4 m s^{-1} seen in Fig. 11 is largely confined to the
443 nocturnal period between 6 PM and 6 AM local time (LT), when the boundary layer is likely to
444 be stable⁸. This period is also largely responsible for the distributional differences between the
445 forecasts and observations noted above. The frequency of relatively larger observed wind speeds at
446 night was sufficient to make the mean bias of forecast/observation pairs to be negative, even though
447 the model generated too few low speed predictions. This may represent a problem with how the
448 model handles the stable boundary layer and its intermittent, localized turbulence (cf. Medeiros and
449 Fitzjarrald 2014, 2015). In contrast, the daytime period of 6 AM to 6 PM LT (panels b and c) seems
450 to be rather well represented in the HRRRV3 forecasts, albeit with a small underrepresentation at
451 higher wind speeds ($\geq 8 \text{ m s}^{-1}$) that also led to small negative net biases.

⁷Precise percentages vary slightly between the station and forecast/observation pair analyses owing to minor data dropouts.

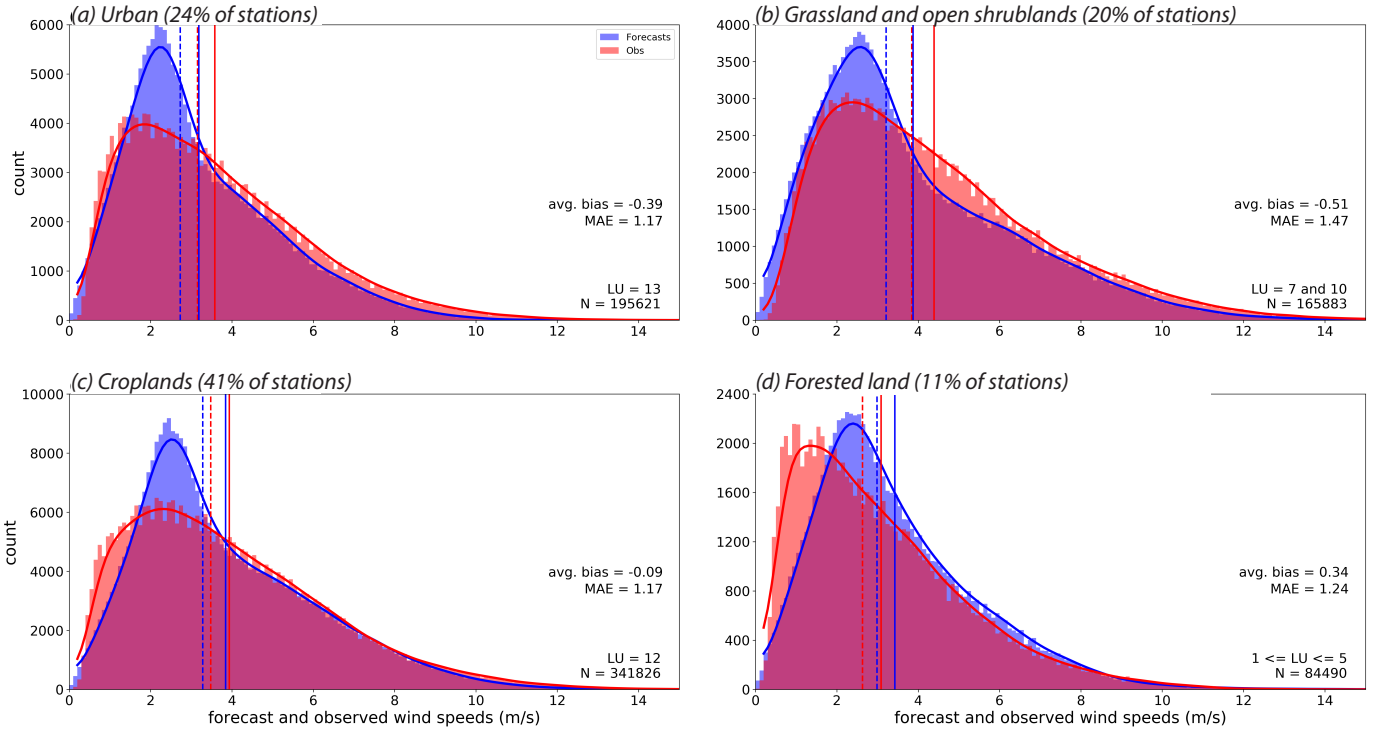
⁸The number of forecast/observation pairs varies among the segments because we are only using the 00 UTC cycle and its 36 h simulations, which means some times have more forecasts than others.

HRRR 00Z cycle ASOS wind bias by primary landuse assignment



415 FIG. 13. Average forecast wind bias (blue bars) aggregated over ASOS stations having same HRRR primary
 416 landuse assignments for (a) April 2019, and (b) April 2021. Red bars represent the weighted contribution
 417 of that class towards the network-average bias. Landuse classes are ordered by weighted bias. Right axis:
 418 percentage of stations having this primary classification. Precise percentages vary slightly between the station
 419 and forecast/observation pair analyses owing to minor data dropouts.

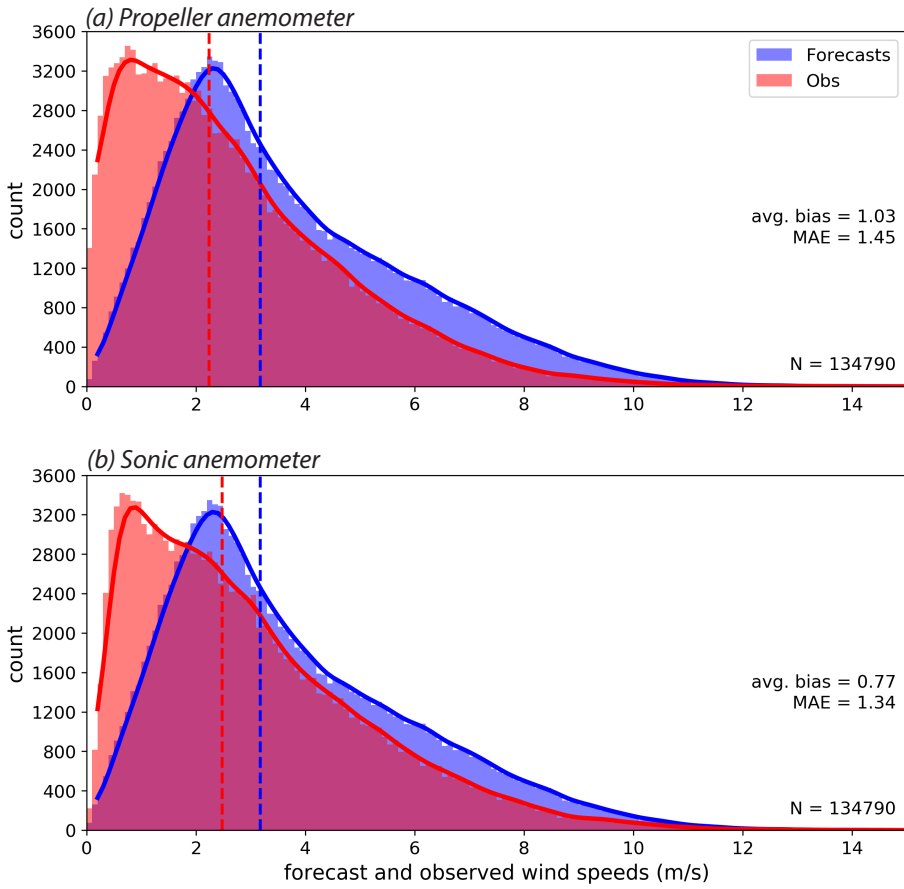
HRRRV3 00Z cycle ASOS histograms by primary landuse assignment: April 2019



427 FIG. 14. Similar to Fig. 11a but segregated by primary landuse (LU) category from the MODIS 21-class
 428 database used by HRRRV3: (a) urban, (b) grasslands and open shrublands, (c) croplands, and (d) forested land
 429 (including deciduous, evergreen, and mixed forest).

452 Those histograms aggregated all landuse classes. Figure 17 focuses on the 6 PM to midnight
 453 LT period differentiated by the landuse groupings examined in Fig. 14. Only the forested lands
 454 (panel d) did not have characteristic underprediction of relatively faster winds, again reflecting
 455 the less than optimal handling of those areas in the model. For the afternoon (noon to 6 PM LT)
 456 period (Fig. 18), however, only the urban classification (panel a) failed to capture the frequency of
 457 stronger winds. Thus, except in the vicinity of cities, the model's inability to capture the frequency
 458 of stronger winds appears to be a nocturnal issue and one that might be addressed by reconsidering
 459 assumptions employed in the stable boundary layer regime. It is surmised that the urban issue
 460 may also stem from overly high specifications of surface roughness in those areas. While many
 461 airports are located in grids designated as urban, that does not mean that the local environment
 462 of the airport is truly city-like. Finally, we reiterate that resolving the issue with forested land or

463 HRRRV3 00Z cycle NYSM histograms: April 2019



471 FIG. 15. Similar to Fig. 11a but for April 2019 wind forecasts for NYSM sites compared to (a) propeller, and
472 (b) sonic observations.

473 removing those stations from the analysis would tend to make the nocturnal underprediction issue
474 appear worse.

467 4. HRRRV4 wind and gust evaluation for April 2021

468 Version 4 of the HRRR became operational on 2 December 2020. The revised model incorporated
469 a number of improvements to the planetary boundary layer and radiation schemes, the land surface
470 model, and numerical methods and diffusion, and adopted a new gravity wave drag treatment
471 (cf. Dowell and co authors 2022). It also shifted to the higher-resolution version of the MODIS

HRRRV3 00Z cycle ASOS histograms by local time: April 2019

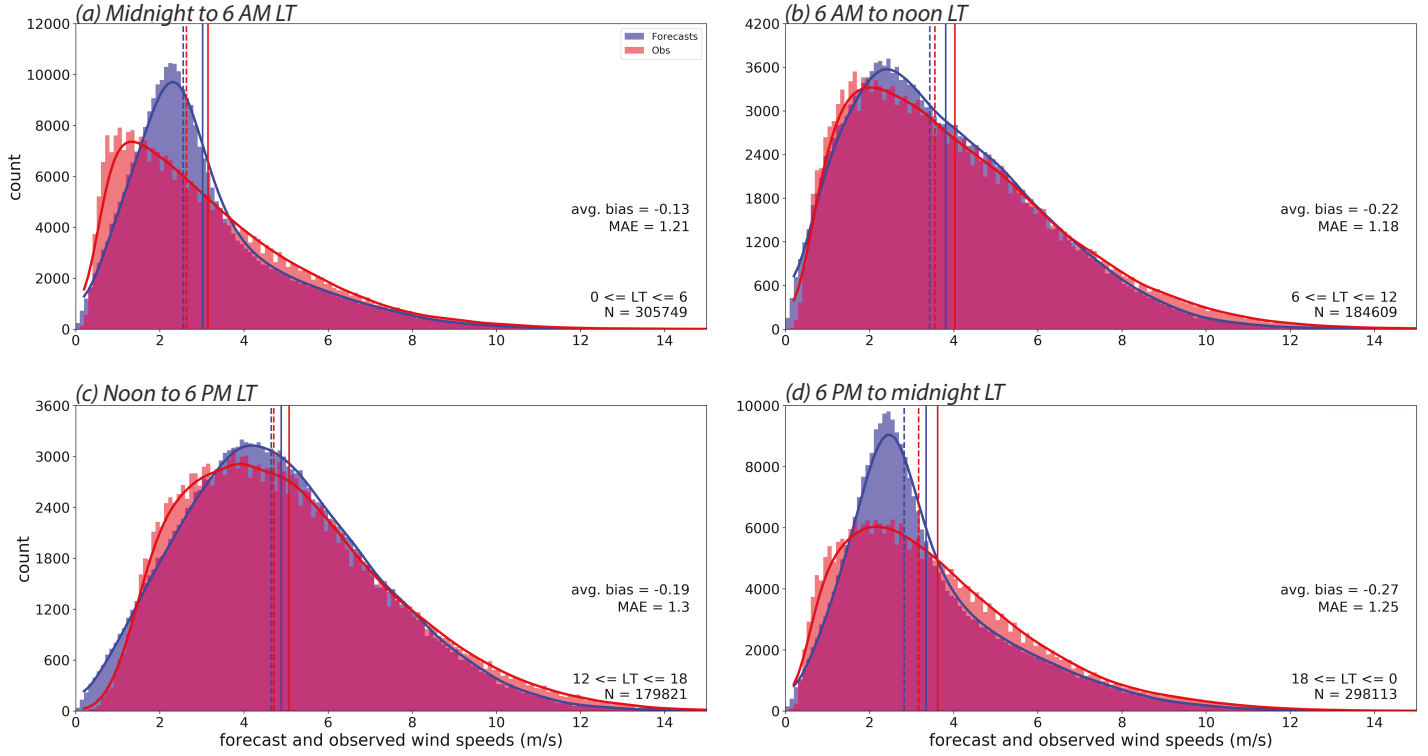


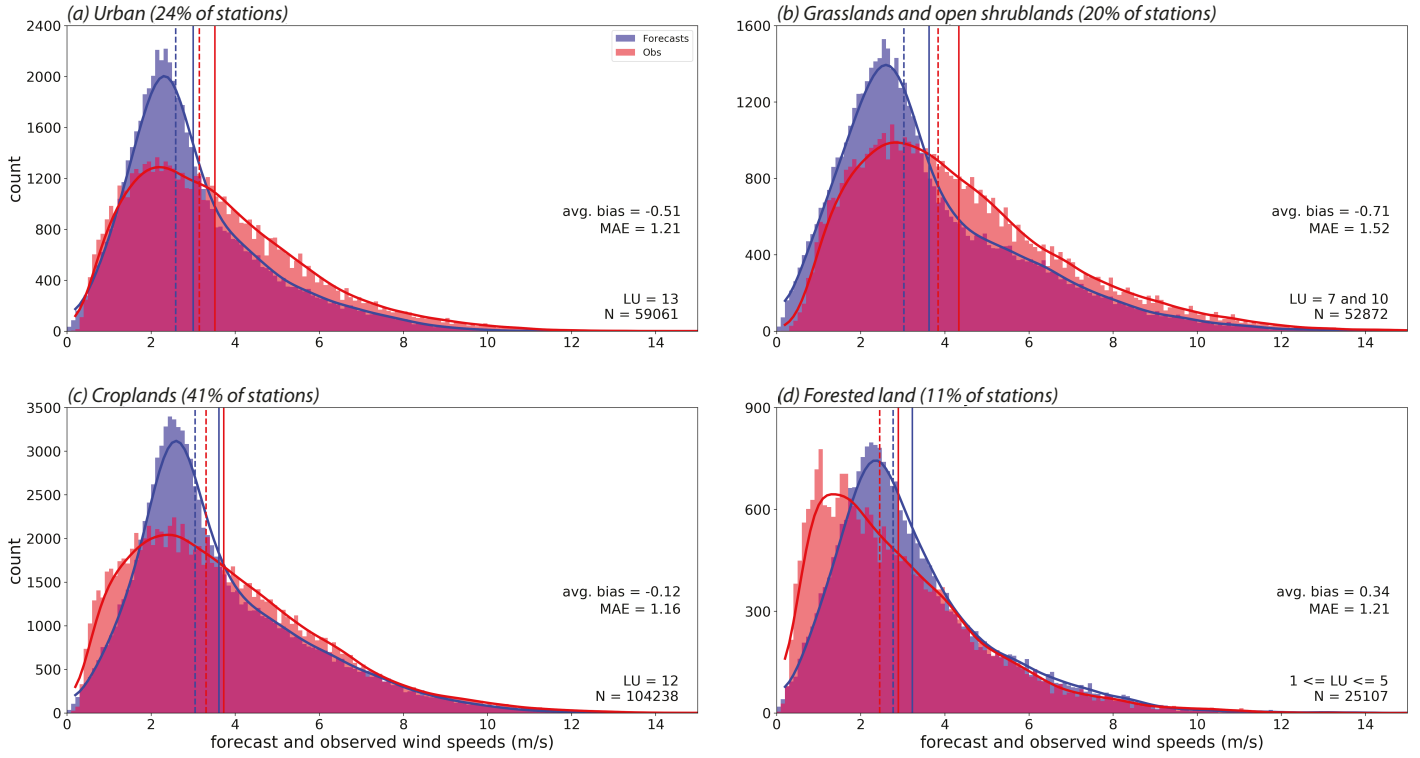
FIG. 16. Similar to Figs. 11a and 14 but segmented with respect to local time (LT).

landuse database that was released with WRF Preprocessing System (WPS) version 3.9 in 2017, with consequences as discussed presently.

Our examination of 10-m wind forecasts at ASOS stations from April 2021 from HRRRV4 emphasizes points of similarity and difference with the April 2019 HRRRV3 results. The verification was again restricted to the 00 UTC cycle and through forecast hour 36, even though V4 now integrates out two full days for that start time. Although not shown, monthly mean wind speeds were very comparable to April 2019 (Fig. 1). Unfortunately, relative to April 2019, there were more missing observations in the ASOS 1-min database in April 2021. As a consequence, the database of hourly mean sustained wind and maximum gust had 32% fewer observations than for April 2019, averaging about 15400 observation/forecast pairs per forecast hour instead of 22650. Only 766 sites remained after removal of misclassified stations and those with 500 or fewer observations. In our judgment, this does not negatively affect the evaluation.

There are more differences between these two MODIS-derived databases than just the resolution enhancement. In HRRRV4 (Fig. 2c), a large fraction of the original croplands class (#12, gold),

HRRV3 00Z cycle ASOS histograms by primary landuse for 6PM-midnight local time: April 2019



465 FIG. 17. Similar to Fig. 16a but focusing on the 6 PM to midnight LT period and separated into different
466 landuse groupings.

486 especially in the eastern CONUS, has been transferred into the previously existing but unused
487 “cropland/vegetation mosaic” group (#14, cyan). The croplands category presently accounts for
488 only 18.3% of ASOS station primary assignments while the mosaic claims 14.9%. In the west,
489 a portion of the open shrublands (#7, maroon) primary assignments have been reassigned as
490 grasslands (#10, light green), constituting 4.3% and 21.0% of ASOS sites in the newer MODIS
491 database, respectively. We have continued combining those landuse types owing to their similarity
492 with respect to model performance. The HRRRV4 grassland area has also spread eastward into
493 the former croplands, so the grassland and open shrubland combination now represented 25% of
494 the April 2021 ASOS primary assignments, an increase of 5 percentage points. Some areas that
495 had been assigned to one of the forest classes (categories 1-5) have been reclassified as woody
496 savannas (#8), increasing its share of the network from 2.6% to 7.2%. Owing to their similarity,

HRRRV3 00Z cycle ASOS histograms by primary landuse for noon-6PM local time: April 2019

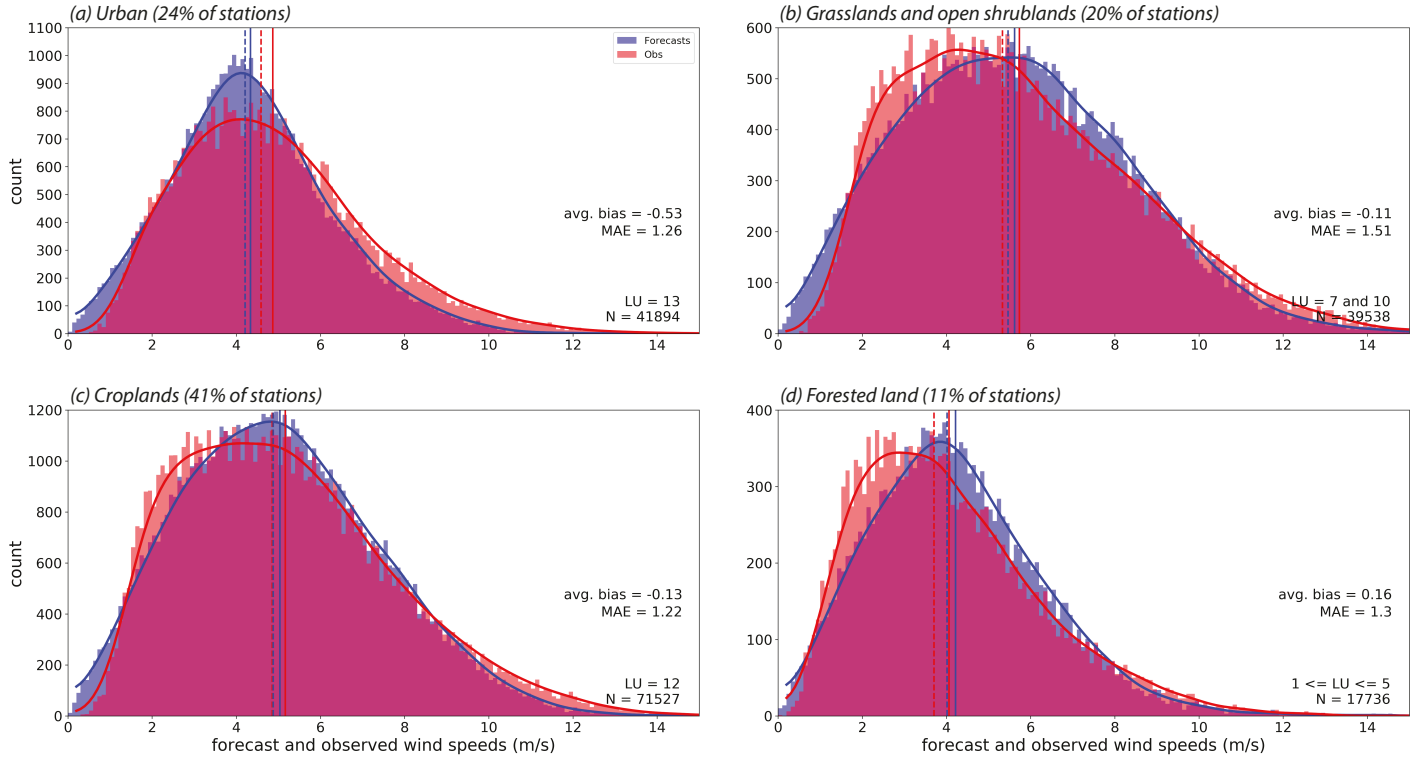


FIG. 18. As in Fig. 17 but focusing on the noon to 6 PM LT period.

497 class 8 was analyzed with the forested land, and this combination represented 13% of the ASOS
498 stations retained in the April 2021 analysis.

499 As in Section 3, above, these are *primary* landuse assignments. The fractional landuse appor-
500 tionments represent another difference with HRRRV3. In HRRRV4, 87% of ASOS stations reside
501 in grid cells assigned more than one landuse class, up from 53% in V3 (compare Figs. 2 panels
502 d and b), a consequence of V4's higher landuse resolution. The average fraction claimed by the
503 primary class was 0.7, a decrease from 0.83 for V3. Again, this was relatively smaller for the
504 forested group and also the new cropland/vegetation mosaic classes (both about 0.6) than for the
505 urban and croplands (both ≈ 0.7) and grasslands (0.8). The HRRRV4 landscape is more finely
506 divided and this makes analyzing by primary landuse assignment less precise, but again we find
507 some value in this effort.

508 Figures 3c and 4c,d present the April 2021 forecast hour analysis. The small negative forecast
509 bias that was previously seen in V3 has vanished (indeed, the mean bias is now essentially zero)
510 although the spatial standard deviation of the forecasts was still smaller than that of the observations

511 at all forecast hours. The local time versions of these figures also revealed some improvements
512 (Figs. 3d and 5c,d). Despite involving fewer sites, the station analysis results and conclusions were
513 little changed. R^2 values for the sustained wind and gust fits were higher for both station-average
514 (Figs. 7c,d) and pairwise (Fig. 10c,d) comparisons and (although not shown, see Gallagher 2021)
515 the average forecast wind was again uncorrelated with bias but the higher wind stations were still
516 underpredicted and lower sites overforecast in a manner that is predictable from iGF or GF⁹. In
517 addition, the association between bias and the difference between forecast and observed temporal
518 standard deviation remained (also not shown, cf. Gallagher 2021). Viewed spatially (Fig. 9d),
519 forecast bias was still concentrated in the east CONUS in general and southeast in particular,
520 although errors were somewhat smaller in magnitude.

521 The wind and gust histograms (Fig. 11c,d) also suggest improvements relative to April 2019.
522 However, the compensating errors between more densely treed areas (the forest and woody savannas
523 categories) and the urban and grassland areas persisted (Fig. 13b). The now more spatially confined
524 croplands class was still the best modeled and the newly separate mosaic group had a positive bias,
525 which is unsurprising because much of the this group's stations are in the southeast, the site of
526 lower wind observations (not shown, but similar to Fig. 1) and positive biases (Fig. 9d). Still, the
527 histograms representing the urban and combined grassland and open shrubland categories (Fig. 19,
528 top row) also reveal better model behavior at relatively higher wind speeds compared to HRRRV3
529 (Fig. 14). For convenience, we have combined the cropland and mosaic classes in Fig. 19c, despite
530 their differences, and note that the forested and woody savanna grouping remained the most poorly
531 handled (Fig. 19d).

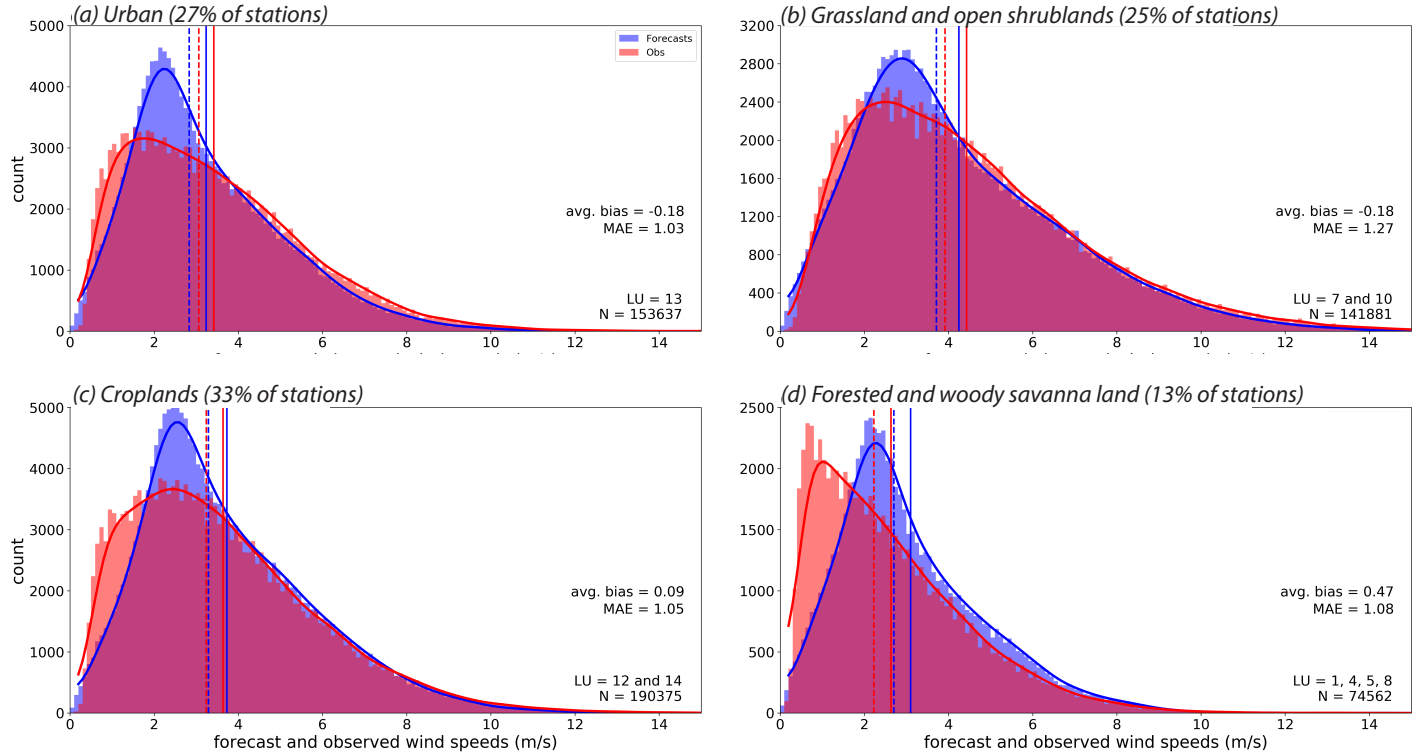
534 In the end, and despite the improvements in model performance, we see that the glaringly different
535 distributional shapes noted previously are still present and that this is still driven by the 6 PM to
536 6 AM period (Fig. 20). Clearly, more work on the stable boundary layer remains to be done.
537 Although 10-m wind speeds during this period are typically not strong, sizable wind errors may
538 have implications for boundary layer pollution transport, wind energy, etc..

539 **5. Summary and recommendations**

540 Our previous study, Fovell and Gallagher (2020, FG20), presented a detailed verification of
541 Version 3 of the HRRR model focusing on surface and boundary layer winds and temperatures. It

⁹Station KDGP, which was an outlier in the April 2019 analysis, did not have sufficient April 2021 observations for inclusion.

HRRRV4 00Z cycle ASOS histograms by primary landuse assignment: April 2021



532 FIG. 19. Similar to Fig. 14, but for April 2021 and referencing primary assignments from the higher resolution
 533 MODIS landuse database used by HRRRV4.

542 was motivated by prior findings of systemic biases in forecast wind speeds at individual locations
 543 even when network-average bias was insignificant (Cao and Fovell 2016; Fovell and Cao 2017;
 544 Cao and Fovell 2018; Fovell and Gallagher 2018). FG20 leveraged underutilized observations (1-
 545 min ASOS and high-frequency radiosonde) to investigate pervasive background biases across the
 546 entirety of the CONUS in the operational HRRR model. The conclusions of FG20 were consistent
 547 with previous work, detailing a pervasive bias in forecasts of surface sustained wind speed that
 548 was highly (negatively) correlated with the observed value itself. Stations having lower average
 549 wind speeds were being overpredicted while the wind threat was being underestimated at windy
 550 locations.

551 The present examination represented a deeper analysis into the nature and cause of these biases
 552 and also covered the now current version, HRRRV4. Analysis enhancements included verification
 553 against hourly mean winds, consideration of local time and landuse classification, inspection of the

HRRRV4 00Z cycle ASOS histograms by local time: April 2021

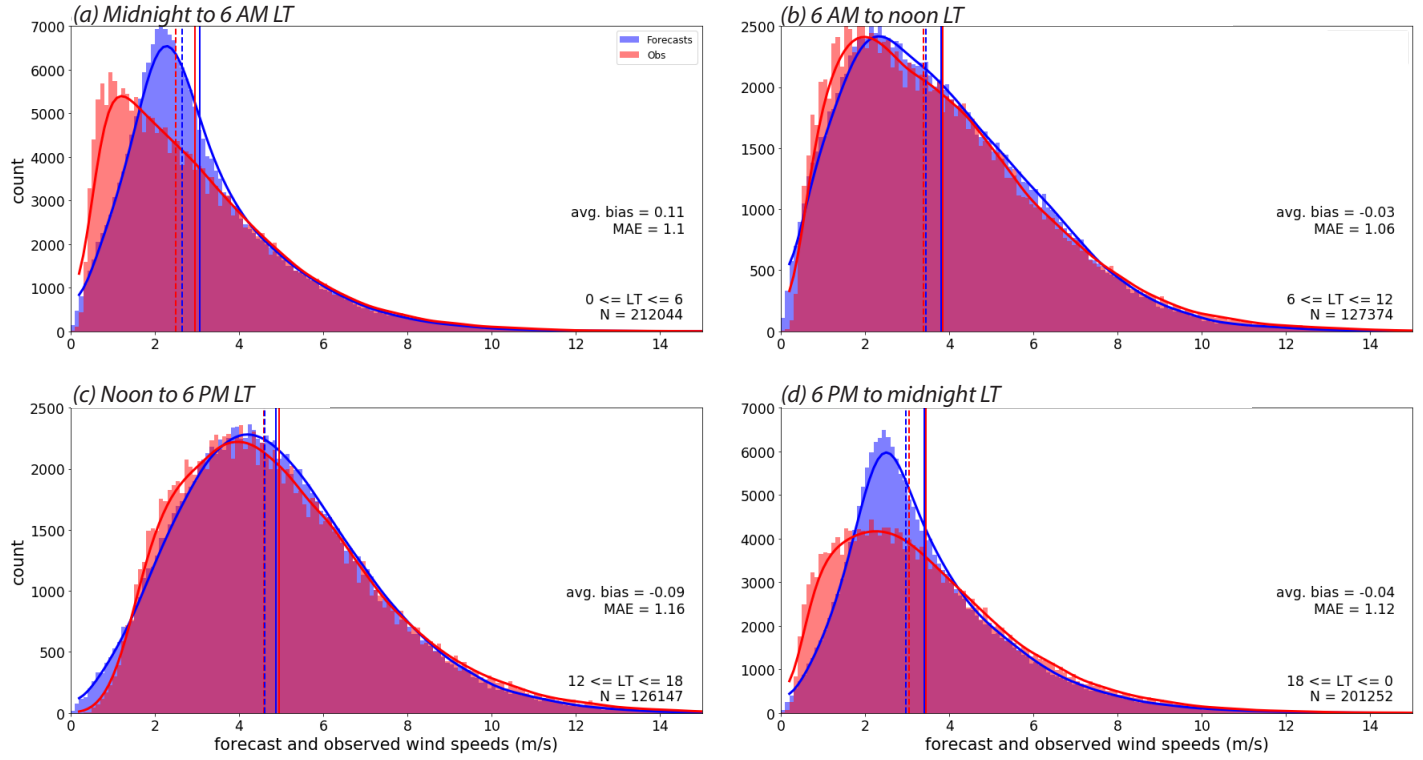


FIG. 20. Similar to Fig. 16, but for April 2021.

554 temporal and spatial variability of forecast and observed winds and biases, and the incorporation of
 555 additional surface observations from the New York State Mesonet (NYSM). Additionally, hourly
 556 maximum gusts were assessed and verified, using the network-average gust factor (GF) approach
 557 as proposed in Cao and Fovell (2018, CF18). Since GF was also correlated with bias, with smaller
 558 and larger factors associated with under- and overprediction, respectively, multiplying the biased
 559 wind forecasts by a fixed value (the network average) was found to reduce the bias in the gust
 560 predictions compared to those of the sustained winds.

561 For two spring months in 2019 and 2021, we showed the network average sustained wind forecasts
 562 for ASOS stations were excellent in Version 3 and even better in the current configuration. That
 563 said, the negative correlation between bias and mean observed wind speed persisted in Version 4,
 564 and we also demonstrated that the forecast and wind distributions were distinctly different overall,
 565 with ASOS forecasts in both versions having less spread about their modal value of about 2.5 m
 566 s^{-1} than in reality. Furthermore, observations associated with below-median GFs skewed towards
 567 higher speeds and those with above-median values skewed sharply leftward, characteristics not

568 captured in the forecasts. The inclusion of stations classified as forested land in the model actually
569 worked to obscure the model's tendency to *underpredict* winds across the bulk of the ASOS
570 network. A large fraction of the NYSM sites are situated in forested areas and that explained why
571 the wind speeds at those stations were substantially overpredicted in the model.

572 Regarding local time, forecast wind distributions during the daytime looked quite good but less
573 so at night, when the boundary and surface layer are usually stable. This demonstrates that further
574 work needs to be done in the nocturnal regime. Even that systemic bias was landscape-dependent,
575 however. Especially in urban and grassland areas, stronger winds at night were more common in
576 the observations than in the model forecasts.

577 Taken together, we see evidence of further improvement in the HRRRV4 relative to its already
578 skillful predecessor, at least in the spring month selected for close analysis. The gust parameteri-
579 zation inspired by Cao and Fovell (2018) continued to work well, despite its simplicity. Because
580 it helped mitigate systemic biases, the CF18 gust can supply a starting point for a more sophis-
581 ticated approach that might also factor in boundary layer depth, winds, and stability for even
582 better-verifying predictions, especially in particularly challenging or dangerous situations (e.g.,
583 downslope windstorms, tropical cyclones, convective storms, etc.). Challenges with respect to the
584 stable boundary layer and the treatment of some landuse classes (especially forested areas) remain.
585 Other important variables, such as temperature, moisture, and the HRRR's own gust potential,
586 have not yet been assessed. These should be foci of future work.

587 *Acknowledgments.* This research depended on support from National Science Foundation grants
588 1450195 and 1921546, the USD/R&E (The Under Secretary of Defense-Research and Engineering),
589 National Defense Education Program (NDEP) / BA-1, Basic Research, SMART Scholarship
590 Program, and Atmospheric Data Solutions LLC.

591 *Data availability statement.* HRRR model outputs can be obtained from Amazon Web
592 Services and Google Cloud as described on the NOAA Big Data Program web page,
593 <https://www.noaa.gov/organization/information-technology/big-data-program>.
594 Versions 3 and 4 of the HRRR are based on the WRF-ARW model available
595 via <https://www2.ucar.edu/wrf/users/>. HRRR model landuse informa-
596 tion was extracted from the WRF model system Geogrid files made available at
597 <https://rapidrefresh.noaa.gov/hrrr/>. One-minute ASOS data are available at
598 <https://www.ncdc.noaa.gov/data-access/land-based-station-data/>. New York
599 State Mesonet data are not publicly available and were used with permission. Mesonet data may
600 be requested at <http://www.nysmesonet.org/weather/requestdata>.

601

APPENDIX

602 In Figs. 16 and 20, we demonstrated that the 10-m wind speed distributions for forecasts and
603 observations were less comparable at night for both versions of the HRRR examined. A reviewer
604 pointed out that our study design incorporated more nighttime than daytime hours and wondered
605 how that influenced the results. We thank the reviewer for alerting us to this. We performed our
606 analyses again, limiting them to forecast hours 0-24, inclusive, which makes the number of night
607 and day hours much more comparable. However, we found few discernible changes to the figures,
608 with the caveat noted below, and there was no impact on our conclusions. As a consequence, we
609 have retained all forecast hours (0-36) common to both HRRR versions for the 00 UTC cycle.

610 The reason for the insensitivity is that many of our analyses involved medians, means, and
611 differences between means (i.e., biases). Even at night, the means and medians of the forecasts and
612 observations were very similar, as were biases and mean absolute errors (Figs. 16 and 20), and that
613 is why removing some of the nocturnal hours did not materially alter the results. The *distributional*
614 differences at night, however, imply larger scatter among forecast/observation pairs. Figure A1 is a
615 version of Fig. 10 in which only pairs for forecast hours 0-24 were retained. Reflecting the reduced

HRRR 00Z cycle ASOS pairwise analysis: April 2019 and 2021 (forecast hours 0-24)

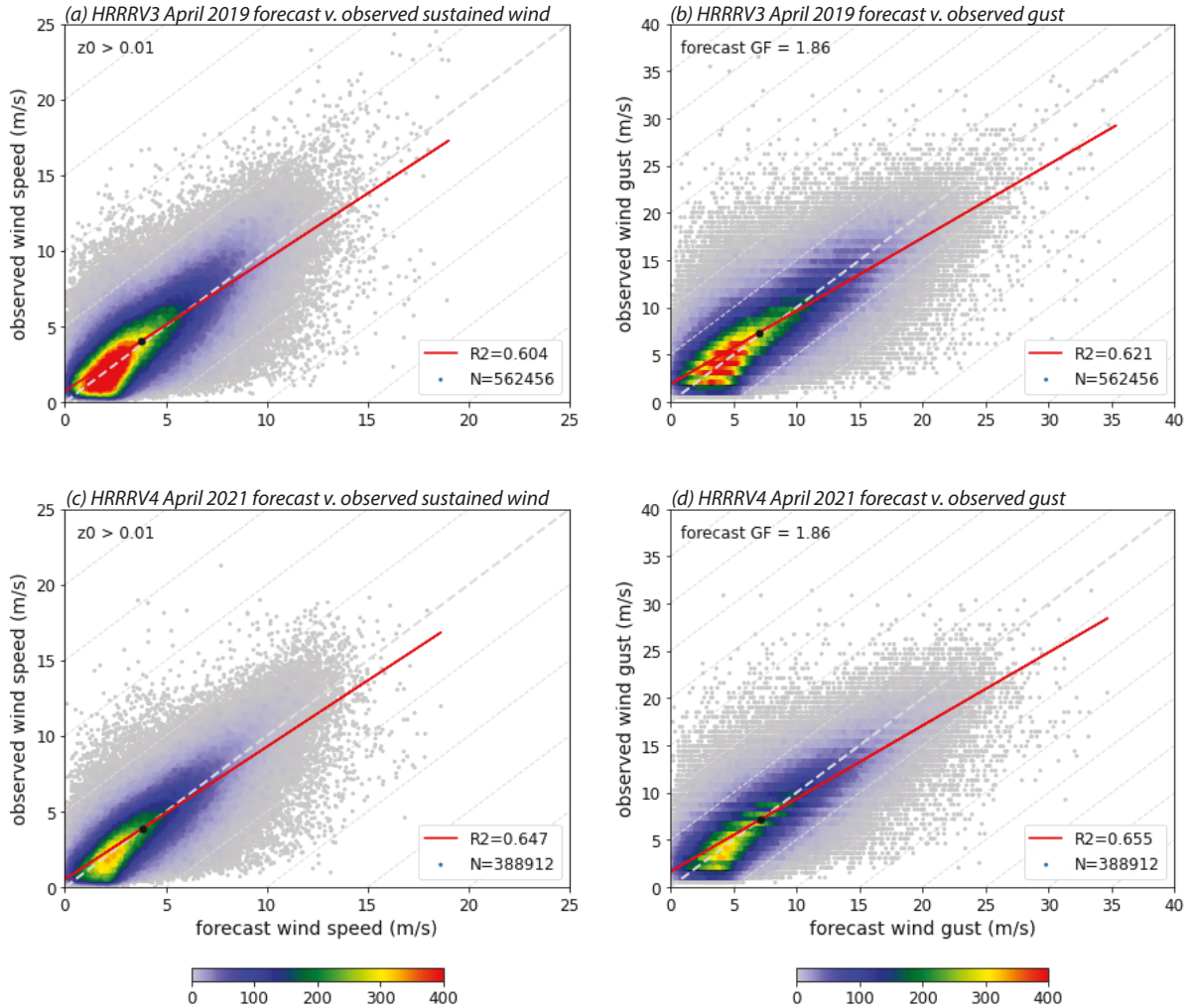


FIG. A1. As in Fig. 10 but for analyses restricted to forecast hours 0-24, inclusive.

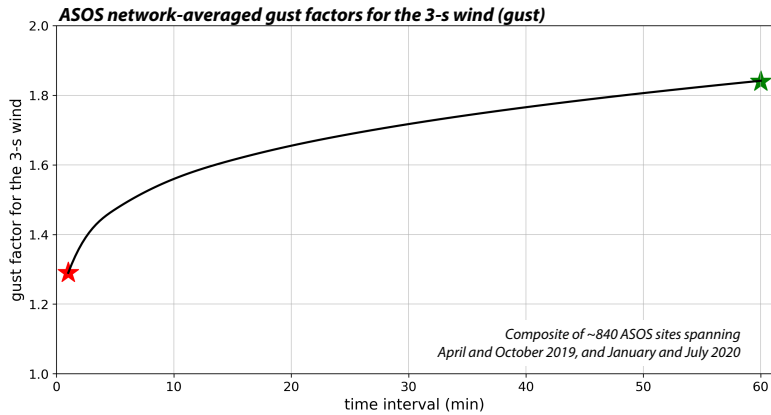
616 scatter, the R^2 values are somewhat higher in this version, but the conclusions from our analyses
 617 remain unchanged.

618 Another reviewer wondered about the large change in gust factor (GF), from 1.29 to 1.86, that
 619 occurred when we shifted from top-of-hour to hourly maximum gusts. First, we note that our
 620 GFs are usually computed as ratios-of-means, such that a station's mean gust is being divided
 621 by its average sustained wind. The network-averaged GF then represents the ratio of the average
 622 of the gusts and sustained winds over all included stations. The mean-of-ratios approach is also

623 valid but typically results in higher gust factors because wind and gust distributions have long tails
624 (cf. Fig. 11 and Gallagher 2021).

625 In previous work (e.g., Fovell and Gallagher 2018), we used ASOS reports from the 1-min
626 database, each of which consisted of a 2-min running average wind (i.e., sustained wind) and the
627 peak 3-sec average (gust) during that one minute interval. Over the ASOS network, the gust factor
628 for the 1-min reports averaged to about 1.29. For this study, we adopted the hourly maximum gust
629 as a better measure of the wind threat. This GF is an hour's fastest 3-s gust report divided by that
630 hour's mean sustained wind, so both the numerator and denominator of the gust factor have been
631 redefined. However, consistent with Harper et al. (2010), the mean wind is nearly the same when
632 averaged over 2- and 60-min periods. Yet, the largest gust discoverable within a given interval
633 logically increases with interval length.

634 Figure A2 presents the ratio-of-means GFs obtained from about 840 ASOS sites vs. the time
635 interval for which the maximum 3-s gust was identified. For each station, for each of four months
636 considered, the station's entire record length T was subdivided into nonoverlapping segments of
637 length τ in minutes, where $1 \leq \tau \leq 60$. Then, for each segment without missing data, the maximum
638 gust report was identified and the mean sustained wind was computed. These were first averaged
639 over all available segments of length τ and then over all stations and the four months, yielding the
640 ratio-of-means network-averaged GF representing time interval τ . Because the average sustained
641 wind for each interval represented the same information, only the numerator of the GF varied
642 among the time intervals. Figure A2 demonstrates that the 1-min GF is about 1.29 (red star) while
643 the 60-min value is about 1.84 (green star), about 1.4 times larger. This curve varies somewhat
644 among seasons and more prominently among networks owing to differences in mean wind speeds,
645 mounting heights, anemometer hardware, characteristic exposures, and possibly other factors, but
646 the shape of the curve is typically logarithmic in time.



647 FIG. A2. Gust factor curve for the ASOS network representing a composite of about 840 stations sampling
 648 four seasons. For each time interval considered, the network-average maximum 3-s wind (gust) was divided by
 649 the network-average sustained wind representing that interval. Red and blue stars represent the one-minute GF
 650 used in Fovell and Gallagher (2018) and the 60-min GF used in this study, respectively.

651 **References**

652 Arya, S., 1999: *Air Pollution Meteorology and Dispersion*. Oxford University Press, 305 pp.

653 Benjamin, S. G., E. P. James, J. M. Brown, E. J. Szoke, J. S. Kenyon, R. Ahmadov, and D. D. Turner,
654 2021: Diagnostic fields developed for hourly updated NOAA weather models. Tech. rep., Earth
655 System Research Laboratory, Global Systems Laboratory, NOAA Tech. Doc. OAR GSL-66,
656 55 pp. <https://doi.org/10.25923/f7b4-rx42>, URL <https://repository.library.noaa.gov/view/noaa/32904>.

658 Benjamin, S. G., and Coauthors, 2016: A North American hourly assimilation and model
659 forecast cycle: The Rapid Refresh. *Mon. Wea. Rev.*, **144**, 1669–1694, <https://doi.org/10.1175/MWR-D-15-0242.1>.

661 Brasseur, O., 2001: Development and application of a physical approach to estimating wind gusts.
662 *Mon. Wea. Rev.*, **129**, 5–25, [https://doi.org/10.1175/1520-0493\(2001\)129\\$<\\\$0005:DAAOAP\\$>\\\$2.0.CO;2](https://doi.org/10.1175/1520-0493(2001)129$<\$0005:DAAOAP$>\$2.0.CO;2).

664 Brotzge, J. A., and Coauthors, 2020: A technical overview of the New York State
665 Mesonet standard network. *J. Atmos. Oceanic Technol.*, **37** (10), 1827 – 1845,
666 <https://doi.org/10.1175/JTECH-D-19-0220.1>, URL <https://journals.ametsoc.org/view/journals/atot/37/10/jtech-d-19-0220.1.xml>.

668 Cao, Y., and R. G. Fovell, 2016: Downslope windstorms of San Diego County. Part I: A case
669 study. *Mon. Wea. Rev.*, **144**, 529–552, <https://doi.org/10.1175/MWR-D-15-0147.1>.

670 Cao, Y., and R. G. Fovell, 2018: Downslope windstorms of San Diego County. Part II: Physics
671 ensemble analyses and gust forecasting. *Wea. Forecasting*, **33**, 539–559, <https://doi.org/10.1175/WAF-D-17-0177.1>.

673 Dowell, D. C., and co authors, 2022: The High-Resolution Rapid Refresh (HRRR): An Hourly
674 Updating Convection-Allowing Forecast Model. Part 1: Motivation and System Description.
675 *Wea. Forecasting*, **XXX**, YYY–ZZZ.

676 Durst, C. S., 1960: Wind speeds over short periods of time. *Meteor. Mag.*, **89**, 181 – 186.

677 Fovell, R. G., and Y. Cao, 2017: The Santa Ana winds of Southern California: Winds, gusts, and
678 the 2007 Witch fire. *Wind Struct.*, **24** (6), 529–564, <https://doi.org/10.12989/was.2017.24.6.529>.

679 Fovell, R. G., and A. Gallagher, 2018: Winds and gusts during the Thomas fire. *Fire*, **1** (3),
680 <https://doi.org/10.3390/fire1030047>.

681 Fovell, R. G., and A. Gallagher, 2020: Boundary layer and surface verification of
682 the High-Resolution Rapid Refresh, version 3. *Wea. Forecasting*, **35** (6), 2255–2278,
683 <https://doi.org/10.1175/WAF-D-20-0101.1>, URL <https://journals.ametsoc.org/view/journals/wefo/35/6/waf-d-20-0101.1.xml>.

685 G. Lufft Mess und Regeltechnik GmbH, 2021: *Technical Data V200A Ultrasonic Wind Sen-*
686 *sor*. Fellbach, Germany, URL <https://www.lufft.com/products/wind-sensors-anemometers-289/v200a-ultrasonic-wind-sensor-2295/productAction/outputAsPdf/>.

688 Gallagher, A. R., 2021: Exploring Environmental and Methodological Sensitivities of Forecasted
689 and Observed Surface Winds and Gusts Using Underutilized Datasets. Ph.D. thesis, University
690 at Albany, State University of New York, 260 pp.

691 Gray, M. E. B., 2003: The use of a cloud resolving model in the development and evalua-
692 tion of a probabilistic forecasting algorithm for convective gusts. *Meteor. Appl.*, **10**, 239–252,
693 <https://doi.org/10.1017/S1350482703003049>.

694 Gutiérrez, A., and R. G. Fovell, 2018: A new gust parameterization for weather prediction models.
695 *J. Wind Eng. Ind. Aerodyn.*, **177**, 45–59, <https://doi.org/10.1016/j.jweia.2018.04.005>.

696 Harper, B., J. D. Kepert, and J. D. Ginger, 2010: Guidelines for converting between various wind
697 averaging periods in tropical cyclone conditions. Tech. rep., World Meteorological Organization
698 Tech. Doc. WMO/TD-1555, 64 pp. URL https://www.wmo.int/pages/prog/www/tcp/documents/WMO_TD_1555_en.pdf.

700 He, S., T. G. Smirnova, and S. G. Benjamin, 2021: Single-Column Validation of a Snow Subgrid
701 Parameterization in the Rapid Update Cycle Land-Surface Model (RUC LSM). *Water Resources
702 Res.*, **57**, e2021WR029955, <https://doi.org/10.1029/2021WR029955>.

703 Holmes, J. D., A. C. Allsop, and J. D. Ginger, 2014: Gust durations, gust factors and gust
704 response factors in wind codes and standards. *Wind Struct.*, **19** (3), 339–352, <https://doi.org/10.12989/WAS.2014.19.3.339>.

705

706 Medeiros, L. E., and D. R. Fitzjarrald, 2014: Stable boundary layer in complex terrain. Part I:
707 Linking fluxes and intermittency to an average stability index. *J. Appl. Meteor. Climatol.*, **53** (9),
708 2196 – 2215, <https://doi.org/10.1175/JAMC-D-13-0345.1>.

709

710 Medeiros, L. E., and D. R. Fitzjarrald, 2015: Stable boundary layer in complex terrain. Part II:
711 Geometrical and sheltering effects on mixing. *J. Appl. Meteor. Climatol.*, **54** (1), 170 – 188,
712 <https://doi.org/10.1175/JAMC-D-13-0346.1>.

713

714 Nakamura, K., R. Kershaw, and N. Gait, 1996: Prediction of near-surface gusts generated by deep
715 convection. *Meteor. Appl.*, **3**, 157–167, <https://doi.org/10.1002/met.5060030206>.

716

717 National Wildfire Coordinating Group, 2019: NCWG Standards for Fire Weather Stations (PMS
718 426-3). National Wildfire Coordinating Group, URL <https://www.nwrg.gov/sites/default/files/publications/pms426-3.pdf>, 46 pp.

719

720 Olson, J. B., J. S. Kenyon, W. A. Angevine, J. M. Brown, M. Pagowski, and K. Suselj, 2019a: *A
721 Description of the MYNN-EDMF Scheme and the Coupling to Other Components in WRF-ARW.*
722 NOAA Technical Memorandum, National Oceanic and Atmospheric Administration, Office of
723 Oceanic and Atmospheric Research, 42 pp., <https://doi.org/10.25923/n9wm-be49>.

724

725 Olson, J. B., and Coauthors, 2019b: Improving wind energy forecasting through numerical weather
726 prediction model development. *Bull. Amer. Meteor. Soc.*, **100**, 2201–2220, <https://doi.org/10.1175/BAMS-D-18-0040.1>.

727

728 Panofsky, H. A., H. Tennekes, D. H. Lenschow, and J. C. Wyngaard, 1977: The characteristics
729 of turbulent velocity components in the surface layer under convective conditions. *Bound.-Lay.
730 Meteorol.*, **11**, 355–361, <https://doi.org/10.1007/BF02186086>.

731

Petersen, E., N. Mortensen, L. Landberg, J. Højstrup, and H. Frank, 1998: Wind power meteorology. Part 1: Climate and turbulence. *Wind Energy*, **1**, 2–22.

732

729 Piccardo, G., and G. Solari, 1998: Closed form prediction of 3-D wind-excited response of slender
730 structures. *J. Wind Eng. Ind. Aerodyn.*, **74-76**, 697–708, [https://doi.org/10.1016/S0167-6105\(98\)00063-4](https://doi.org/10.1016/S0167-6105(98)00063-4).

731

732 Pichugina, Y. L., and Coauthors, 2019: Spatial variability of winds and HRRR–NCEP model error
733 statistics at three Doppler-lidar sites in the wind-energy generation region of the Columbia River
734 Basin. *J. Appl. Meteor. Climatol.*, **58**, 1633–1656, <https://doi.org/10.1175/JAMC-D-18-0244.1>.

735 R.M. Young Company, 2000: *Meteorological Instruments Instructions Wind Monitor-HD*
736 *Model 05108*. Traverse City, MI, USA, URL https://s.campbellsci.com/documents/ca/manuals/05108-10_man.pdf.

737

738 Rolinski, T., S. B. Capps, R. G. Fovell, Y. Cao, B. J. D'Agostino, and S. Vanderburg, 2016: The
739 Santa Ana wildfire threat index: Methodology and operational implementation. *Wea. Forecasting*, **31**, 1881–1897, <https://doi.org/10.1175/WAF-D-15-0141.1>.

740

741 Rolinski, T., S. B. Capps, and W. Zhuang, 2019: Santa Ana winds: A descriptive climatology.
742 *Wea. Forecasting*, **34 (2)**, 257 – 275, <https://doi.org/10.1175/WAF-D-18-0160.1>, URL https://journals.ametsoc.org/view/journals/wefo/34/2/waf-d-18-0160_1.xml.

743

744 Sheridan, P., 2011: Review of techniques and research for gust forecasting and parameterisation forecasting. Tech. rep., UK Meteorological Office Research Technical Report 570., 64 pp. URL https://www.researchgate.net/profile/Peter-Sheridan-2/publication/268744498_Review_of_techniques_and_research_for_gust_forecasting_and_parameterisation/links/5474c0b00cf245eb436e0791/Review-of-techniques-and-research-for-gust-forecasting-and-parameterisation.pdf.

745

746

747

748

749

750 Skamarock, W. C., and Coauthors, 2019: A description of the Advanced Research WRF version
751 4. Tech. rep., NCAR Technical Note NCAR/TN-556+STR, Boulder, CO, 145 pp. URL https://www2.mmm.ucar.edu/wrf/users/docs/technote/v4_technote.pdf.

752

753 Stucki, P., S. Dierer, C. Welker, J. J. Gómez-Navarro, C. C. Raible, O. Martius, and S. Brönnimann,
754 2016: Evaluation of downscaled wind speeds and parameterised gusts for recent and historical
755 windstorms in Switzerland. *Tellus A: Dynamic Meteorology and Oceanography*, **68 (1)**, 31 820,
756 <https://doi.org/10.3402/tellusa.v68.31820>.

757 Westerling, A. L., D. R. Cayan, T. J. Brown, B. L. Hall, and L. G. Riddle, 2004: Climate, Santa
758 Ana winds and autumn wildfires in Southern California. *Eos, Trans. Amer. Geophys. Union*, **85**,
759 289–296, <https://doi.org/10.1029/2004EO310001>.

760 Wilczak, J. M., and Coauthors, 2019: The Second Wind Forecast Improvement Project (WFIP2):
761 Observational field campaign. *Bull. Amer. Meteor. Soc.*, **100** (9), 1701–1723, <https://doi.org/10.1175/BAMS-D-18-0035.1>.

763 WMO, 2018: Guide to Meteorological Instruments and Methods of Observation. WMO no. 8,
764 Geneva, Switzerland. World Meteorological Organization, URL https://library.wmo.int/index.php?lvl=notice_display&id=12407#.YWR0VC-B17h, 1177 pp.
765